Magneto-photoluminescence of GaAs/AlxGa1-xAs quantum dots

Schildermans, Nele

Award date:
2004

TU/e Technische Universiteit Eindhoven

Katholieke Universiteit Leuven

Magneto-photoluminescence of $GaAs/Al_xGa_{1-x}As$ quantum dots

Nele Schildermans

Promoters:
Prof. B. Koopmans
Prof. V.V. Moshchalkov
Dr. M. Hayne

2004

Abstract

Novel GaAs/$Al_xGa_{1-x}As$ quantum dots (QD), produced by combining self-assembly and strain-enhanced etching into a single-stage process are studied. The resulting quantum dot/well system is practically unstrained, with a good size homogeneity and negligible intermixing at the interfaces, which makes it an interesting system for the investigation of fundamental properties of QDs. The optical properties of these novel quantum structures are studied here by photoluminescence (PL) in magnetic fields up to 50 T. This method gives information about the confinement and exciton properties in the plane perpendicular to the applied field. Both the quantum well and the QD PL peaks are studied with the field applied either parallel or perpendicular to the growth direction. The exciton mass is found to depend inversely on the structure size, due to the non-parabolicity of the energy band. The excitons are weakly confined in these structures and the electrons can even tunnel out in some cases. Furthermore, QD excited states are measured and investigated as function of the magnetic field.

Acknowledgements

I would like to thank everyone, who helped me during this traineeship and made it possible for me to write the thesis. First of all thanks to Prof. Victor Moshchalkov of the KULeuven for giving me the opportunity to do this traineeship in the Pulsed Field Group. Many thanks to my promoter Prof. Bert Koopmans from the TU Eindhoven to support this project.

I especially want to thank Dr. Manus Hayne for his useful advice and encouragement. The many discussions truly helped me understanding the subject and interpreting the results. Thanks also to Stefanie Godefroo and Jochen Maes for their practical assistance during the measurements.

Thanks to Dr. A. Rastelli and Dr. O. G. Schmidt of the Max Planck Institut für Festköperforschung in Stuttgart for making the samples.

And of course, thanks to all the people of the Pulsed Field Group for the pleasant ambience in the laboratory.

Contents

1 Introduction

Semiconductors heterostructures are studied a lot for technological applications and interesting fundamental physics. The main characteristics of semiconductors are the minimum band gap and the lattice constant. A wide variety of structures with tuneable properties can be produced by combining semiconductors with different characteristics. Downscaling such structures from bulk to nanosize, will change the electronic and optical properties, because confinement phenomena will start to play a role. These phenomena are not only interesting from the fundamental point of view, but can also be applied in electronic and opto-electronic devices.

1.1 Semiconductor quantum structures

Semiconductors are combined into heterostructures to make devices with specific properties, which are in general determined by the difference between the band gaps. The differences in conduction and valence bands can form a potential well or barrier for the electrons and the holes. A potential well can be made by surrounding a semiconductor layer (with a small band gap) by a barrier material with a larger band gap. Depending on the band offsets, the middle layer will form a potential well for either one or both of the charge carriers. Structures that confine both types of charge carriers are called type-I structures. When only one type of the charge carriers is confined, then we talk about a type-II system. A type-III structure is in between these both cases, which means that there is no barrier for one of the charge carriers [1].

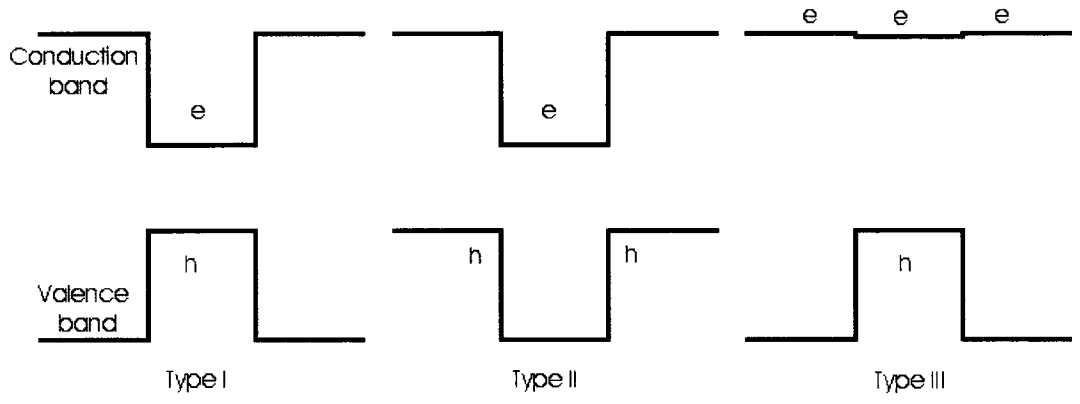

Figure 1: Three different types of heterostructures can be produced, by using semiconductors with different band gap. The first type confines the electrons and the holes in the same part of the heterostructure, while in a type-II structure there is a potential well for one type of charge carriers and a barrier for the others. A type-III system is in between the other two types, with no barrier for one of the charge carriers.

When the thickness of the potential well is comparable to the de Broglie wavelength of the electron, then quantum phenomena can occur. The thin layer is then called a quantum well (QW). The charge carriers are restricted in their movements by the QW in the direction perpendicular to the QW and this confinement causes a discretisation of the energy levels in this direction. The charge carriers can move freely in the plane of the well, so in these two directions the energy can vary continuously. This means that for each discrete energy state in the one direction, there is a continuous band in the other directions. The discretisation of the energy levels as a consequence of the decreasing dimensions of a structure is discussed in more detail in chapter 2.

A QW is called a two-dimensional (2D) structure, because the thickness is very small in comparison with the other two directions. Also 1D or 0D structures can be made, which are called quantum wires or quantum dots (QD) respectively. These last structures can be produced by self-assembly, using materials with a different lattice constant. The self-assembling principle and other production methods of these structures are explained in more detail in chapter 3.

1.2 Applications

Semiconductor nanostructures are studied a lot for their electronic and optical properties, which are used already for diverse applications. This nanotechnology makes it possible to develop always smaller electronic devices, *e.g.* the tunnel diode. Also the optical properties are interesting for applications, for instance lasers, which are discussed here. A lot of research is done on QD lasers, because the expectation is that their properties are in general better than bulk and QW semiconductor lasers. It is already demonstrated that QD lasers have a higher efficiency and a better temperature stability [2, 3] as a result of the total quantisation of the energy levels and the densities. The threshold current, needed to start the lasing process and an important property of lasers, is lower for the QDs. Another advantage of the QD lasers is the lower chirp, *i.e.* the change of emission wavelength with high frequency on/off operation [4]. The expectation is that these lasers will have a better lifetime and are less sensitive for impurities in the material, so the design is more robust [5].

Lasers are used already a lot for several applications such as data storage and transport. Telecommunication is becoming more important in everyday life, stimulating research to make data transport faster and cheaper. The optical transport of data by fibre bundles is such a fast way and QD lasers could be very useful for this application. However, one of the problems of optical transport is the light absorption in the fibres. Certainly when large distances should be spanned, then more amplifiers are needed, which makes the data transport more expensive. The glass fibres that are used for optical communication have the lowest absorption at a wavelength of 1.3 μm or 1.55 μm. The aim of a lot of research is thus to make a QD laser with these specific wavelengths. It is already possible to make QD lasers with a wavelength of 1.3 μm.

1.3 An unstrained GaAs/$Al_xGa_{1-x}As$ quantum structure

Here, we studied GaAs/$Al_xGa_{1-x}As$ quantum structures, which are produced by A. Rastelli and O.G. Schmidt of the Max Planck Institute für Festköperforschung in Stuttgart [6]. They developed a new method to make these novel type of QDs, using self-assembly as a patterning of the substrate surface. In contrast with most patterning methods, this production process happens completely *in situ* by using a molecular beam epitaxy set-up with an etching unit. Self-assembly can't be used directly in this case, because GaAs and $Al_xGa_{1-x}As$ have almost the same lattice constant (0.3% mismatch for GaAs/AlAs). This implies that this type of QDs is unstrained and that there is no intermixing at the interfaces.

Strain and intermixing influence the band structure and thus the optical properties in most self-assembled dots. Strain causes deformation of the bandstructure. This implies that the energies and the curvatures of the bands change. Strain also increases the anisotropy of the lattice, and so the anisotropy of the optical and electronic properties. Intermixing changes the composition of the dots, especially at the edges, which also influences the energy bands and the strain in the structure [1].

So, we expect that the absence of these two effects will simplify the understanding of the optical properties of these structures. It is then possible to study only the confinement effect due to the decreasing dimensions. These advantages in combination with the fact that GaAs and $Al_xGa_{1-x}As$ are both very well-known materials make this structure an excellent candidate for a model system, which can be used to study the fundamental properties of QDs. Furthermore, the shape of the QDs is well known with this production method, which is interesting for calculations on this system. In principle it is possible to do detailed calculations with no structural adjustable parameters, because of the good knowledge of all aspects of the samples. So, it will be possible to compare the experimental results of this research with calculations, which is an important motivation to study these samples. Such work is currently in progress in collaboration with A. Schliwa of the Technical University of Berlin.

These structures are interesting from the fundamental point of view, but can also be interesting for applications. The properties of quantum dots depend in general on the production method. Unstrained dots with the same the size homogeneity as self-assembled dots can be produced with this method, as evidenced by the narrow PL line widths. So, the advantages of self-assembly and a GaAs/AlGaAs system are combined in these dots.

The optical properties are studied by using magneto-photoluminescence technique, which is explained in chapter 4. This method gives information about the properties, *i.e* .the mass and the radius, of an electron-hole pair. The discussion of the experimental results follows in chapter 5.

2 Magneto-photoluminescence on low dimensional structures

2.1 From bulk to quantum dot

As already mentioned briefly in the introduction, when the dimensions of a structure become small enough, then quantum mechanical phenomena occur. For bulk semiconductors the energy bands are continuous and the density of states changes also continuously as function of the energy. When the dimensions of the structure are smaller than the de Broglie wavelength, then the electron can't move freely through the crystal structure. The expression for the de Broglie wavelength is given in equation (2.1) and depends on the mass and the temperature.

$$\lambda = \frac{h}{p} = \frac{h}{\sqrt{2m^* kT}} \tag{2.1}$$

In this equation is p the momentum of the electron, h Planck's constant, k Boltzmann's constant and m^* the effective mass, which depends on the material. kT is here the thermal energy. This expression is valid in a pure semiconductor, where the charge carriers are only thermally excited. This wavelength is in general much larger than the lattice constant, which means that structures with a size of several lattice constants can already be a quantum structure. The quantum behaviour of the electrons means that the energy states are no longer continuous, but discrete. Also the density of states changes from a continuous behaviour in bulk to a sum of delta functions for a 0D system, as illustrated in Figure 2 [1, 7].

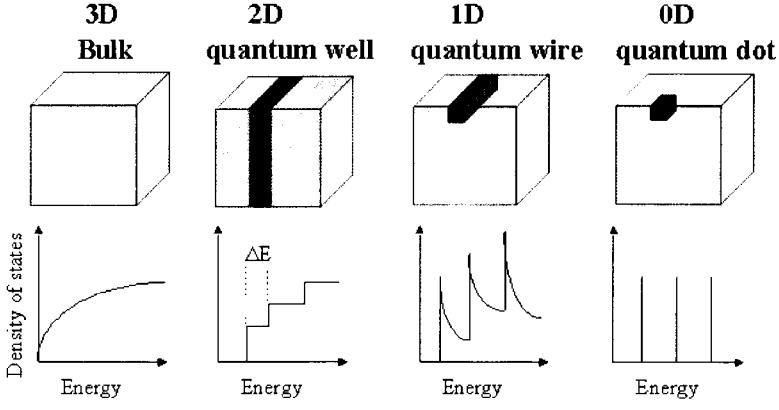

Figure 2: The density of states changes from a continuous behaviour in bulk material to a step function for a 2D system and finally to a sum of δ-functions for a 0D system.

It is this change in density of states that makes quantum structures interesting for laser applications. In a bulk system the density of states goes to zero for the lowest energy state, while in a quantum well a finite number of electrons can sit in the lowest possible energy state. The total discretisation of the energy levels in the case of the QDs implies that electrons in the lowest energy state need a finite

amount of energy, more than the thermal energy kT, to be exited in a higher energy state. It is this property that causes the increase of the optical gain of QD lasers and makes them insensitive to temperature.

We will now describe the discretisation of the energy levels starting from an electron in bulk material. An electron in bulk material can be treated as a free electron with electron mass replaced by an effective mass. This effective mass is already used in equation (2.1) and is an approximation to take into account the influence of the periodic lattice on the charge carrier. This description is called the effective mass approximation and electron energy is now given by

$$E_{3D} = \frac{\hbar^2}{2m^*}\left(k_x^2 + k_y^2 + k_z^2\right). \tag{2.2}$$

For a hole, the same expression is valid, but the electron effective mass has to be replaced by the hole effective mass. When the electron (or hole) is confined, for instance, in the z-direction, then the energy of the electron becomes

$$E_{2D} = \frac{\hbar^2}{2m^*}\left(k_x^2 + k_y^2\right) + E_{n,z}. \tag{2.3}$$

The discrete energy $E_{n,z}$ is the solution of the Schrödinger equation, which is in the case of an infinitly deep potential square well

$$E_{n,z} = \frac{\hbar^2}{2m^*}\left(\frac{n\pi}{l_z}\right)^2 \quad with\ n = 1,2,3,... \tag{2.4}$$

This energy is called the confinement energy and depends on the thickness l_z of the QW, n is the principle quantum number. The density of states for a 2D system is a step function, with steps at the energies $E_{n,z}$. The density of states is constant between these steps. A charge carrier is localized in three directions in the QD, which causes discrete energy states in three directions. The density of states is now a sum of δ-functions: the energy states don't form bands in the k-space, but are now discrete points [1].

The confinement energy in equation (2.4) is a theoretical expression for the case of an infinitly deep potential well. In real structures the potential well is never infinitly deep and this equation is just an approximation. When the quantum well is smaller, then the confinement energy is higher. In theory this confinement energy increases to infinity when the thickness decreases to zero. For a real quantum well there is a maximum confinement energy. When the quantum well is too small, then the confinement energy increases above the barriers and the electrons will no longer be confined. The wavefunction will spill over into the barriers, the electrons can leak out, and the energy level of the electrons goes down again.

2.2 Photoluminescence

Photoluminescence is a light absorption and emission process, which is used here to obtain information about QD properties. When light shines on a semiconductor, then the material may absorb the light. This means that an incident photon hits an electron in the valence band and transfers its energy to the electron. The electron is excited into the conduction band, which is process 1 in Figure 3. A hole stays behind in the valence band. This process happens at constant k-value, which means that the momentum of the electron doesn't change. Not all the photons that hit an electron will be annihilated. The photon must have enough energy (at least the band gap at the k-value of the electron) and there must be a free place in the conduction band at the same k-value. The next step in this photoluminescence process is the relaxation of the electron to the bottom of the conduction band. The hole relaxes to the top of the valence band (step 2 in Figure 3). The electron lowers its energy during relaxation by the phonon interaction with the lattice, which is a non-radiative process. Also the momentum (and thus the k-value) of the electron changes by emission of a phonon. The bottom of the conduction band and the top of the valence band are at the same k-value in a semiconductor with a direct band gap. This means that radiative recombination is possible (step 3 in Figure 3). The released photon would have an energy equal to the band gap.

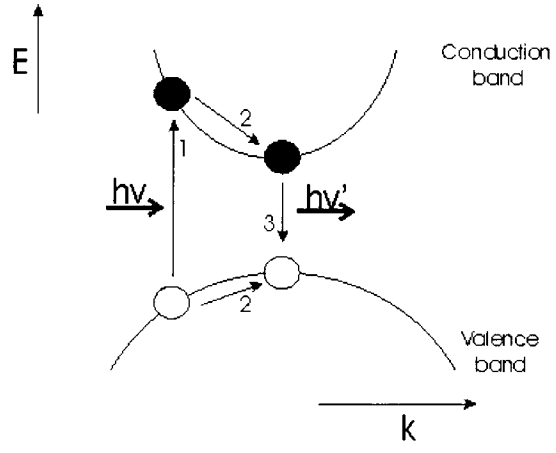

Figure 3: The photoluminescence process consists of three steps. First an electron is excited from the valence band into the conduction band by absorption of a photon (1). Then the electron and the hole relax to the bottom and the top of the conduction and the valence band respectively (2). In the third step (3) the electron and the hole recombine resulting in the radiation of a photon.

The relaxation process in a quantum structure means that the electrons, which are excited in the barrier material, will move to the lower conduction band in the quantum structure. This results in a high concentration of electrons and holes in the quantum structure that recombine there and radiate photons with an energy that depends on the structure size and the material [1].

The energy of this radiated photon is found from a photoluminescence measurement and this gives information about the material. The measured photon energy can be lower than the band gap, certainly in bulk semiconductors, since before the recombination the electron and the hole can lower their total energy by forming an exciton, a bound electron-hole pair. This is possible because of the Coulomb attraction between the opposite charges. The Coulomb potential is

$$V = \frac{-e^2}{4\pi\varepsilon\sqrt{\langle \rho^2 \rangle}}. \tag{2.5}$$

Here is ε the electric permittivity of the semiconductor material and $\langle \rho^2 \rangle^{1/2}$ the average distance between the electron and the hole, which is called the exciton radius. This Coulomb binding energy is

$$E_{binding} = \frac{Ry^*}{n^2} \quad with\ Ry^* = 13.6eV\frac{\mu}{m_0\varepsilon^2} \quad and\ \mu = \frac{m_e^* m_h^*}{m_e^* + m_h^*}. \tag{2.6}$$

In this equation Ry^* is the effective Rydberg binding energy and n is the principle exciton quantum number, μ is the reduced effective mass. The binding energy depends inversely on the distance between the electron and the hole, so it is higher for an exciton in a quantum structure.

The total energy of the exciton is now the sum of the electron and the hole energy minus the Coulomb binding energy as given in equation (2.7), and this is also the measured photon energy.

$$E = E_e + E_h - E_{binding} \tag{2.7}$$

Other factors can have an influence on the measured photoluminescence spectrum, for instance, the presence of impurities, which behave as donors or acceptors. An excess of one type of charge carriers can cause band bending and the formation of charged excitons, which makes the situation more complicated.

2.3 The influence of the magnetic field

An applied magnetic field will influence the energy of an exciton and so the luminescence energy. In fact the magnetic field causes a magnetic confinement, which will deform the electron and the hole wavefunction due to the Lorentz forces. This causes a Zeeman splitting of the energy levels into Landau levels. The expression for these energy levels is given by

$$E_n = \left(n + \frac{1}{2}\right)\hbar\omega_c \quad with\ \omega_c = \frac{eB}{\mu}\ and\ n = 0,1,2,... \tag{2.8}$$

The electron and the hole interact by Coulomb attraction to form an exciton. The exciton energy is also influenced by the confinement of the quantum structure. When the exciton is put in a magnetic

field, then the magnetic interaction will compete with the Coulomb interaction and the spatial confinement [7, 8].

The influence of the magnetic field is approximated as a perturbation on the exciton energy as long as the Coulomb binding energy is bigger than the magnetic cyclotron energy [8]. The spatial confinement is indirectly taken into account in this approximation because the Coulomb binding energy depends on the spatial confinement. It is found that the exciton energy has a parabolic dependence on the magnetic field [9, 10]:

$$E = E_0 + \frac{e^2 \langle \rho^2 \rangle}{8\mu} B^2 \tag{2.9}$$

E_0 is the exciton energy at zero field, given by equation (2.7).

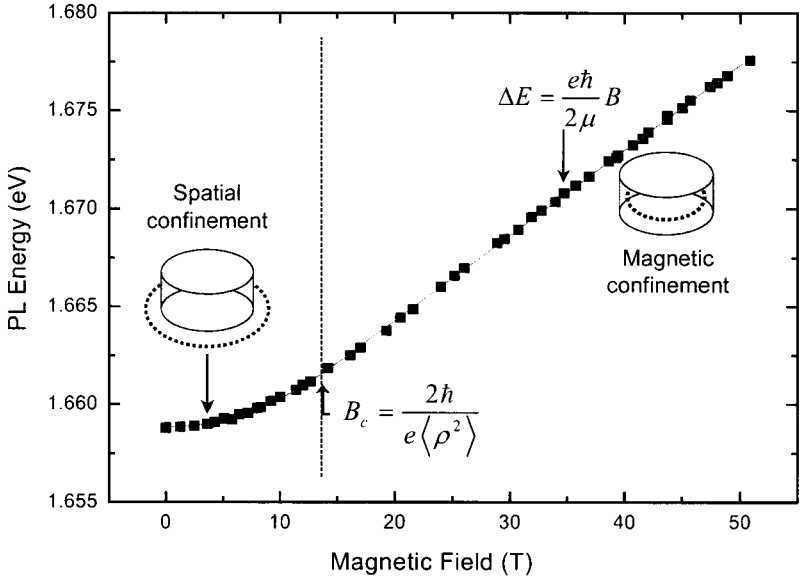

Figure 4: An example of a magneto-photoluminescence measurement. The crossover from parabolic to linear behaviour happens when the magnetic confinement overcomes the spatial confinement. The value B_c gives information about the exciton radius. The slope of the linear part depends on the exciton mass.

At higher fields the magnetic confinement overcomes the Coulomb confinement and equation (2.9) is no longer valid. The magnetic field crushes the exciton wavefunction smaller than its original extent, the exciton energy will depend linearly on the magnetic field, parallel to the first Landau level, and is given by

$$\Delta E = \frac{\hbar e B}{2\mu} \tag{2.10}$$

The energy of the exciton is now the sum of the energies of the confined electron and hole increased with the energy of the lowest Landau level. The Coulomb binding is small in comparison to the magnetic confinement and can be ignored in high fields. The reduced exciton mass can now be determined from the slope of the energy as function of the magnetic field. Note that effects such as spin splitting in a magnetic field are not taken into account in this model. This would cause a splitting of each Landau level in two levels. In most cases this effect is small and not measured, so it can be ignored, but this means that the calculated mass is an approximation.

There are now two different regimes for the exciton energy in a magnetic field, with a crossover regime in between where the magnetic confinement equals the sum of the spatial and Coulomb confinement. This crossover is here approximated by the assumption that there is a strict transition from parabolic to linear behaviour at a certain field value, called the crossover field B_c. The model used here to describe the exciton energy in fields combines the equations of the two regimes into one function supposing that this function should be continuous and have a continuous derivative. So for small fields up to B_c, the exciton energy can be expressed by

$$E = a_1 + a_2 B^2 \tag{2.11}$$

For large fields the energy shift is linear and the data is analysed by

$$E = a_3 + a_4 B \tag{2.12}$$

So there are five parameters (a_1, a_2, a_3, a_4 and B_c) in this model that can be reduced to three by imposing the mentioned boundary conditions, giving

$$\begin{aligned} a_3 &= a_1 - a_2 B_c^2 \\ a_4 &= 2 a_2 B_c \end{aligned} \tag{2.13}$$

Comparing now the equations (2.11) and (2.12) with the equations (2.9) and (2.10), then it becomes clear that the three remaining parameters are related to the zero field luminescence energy, the exciton mass and radius. The single function to describe exciton energy then becomes

$$\begin{aligned} E &= E_0 + \frac{e^2 \langle \rho^2 \rangle}{8\mu} B^2 \qquad & for\ B < B_c = \frac{2\hbar}{e\langle \rho^2 \rangle}, \\ E &= E_0 - \frac{\hbar^2}{2\mu \langle \rho^2 \rangle} + \frac{\hbar e B}{2\mu} \qquad & for\ B < B_c = \frac{2\hbar}{e\langle \rho^2 \rangle}. \end{aligned} \tag{2.14}$$

The crossover happens at the field value B_c, which depends only on the exciton radius and not on the exciton mass. The change of a parabolic behaviour to a linear dependence occurs when the magnetic length l_B becomes of the order of the exciton radius:

$$\frac{\langle \rho^2 \rangle^{1/2}}{\sqrt{2}} = l_B \quad with\ l_B = \sqrt{\hbar / eB}\ . \tag{2.15}$$

This model gives information about the exciton radius and the exciton mass. Of course the assumption that the crossover from parabolic to linear regime happens at one specific field value is a hard approximation. Other models are available that use an interpolation between the two regimes, but a comparison of these different models by Maes [7] proved that they give similar results.

The magnetic field has only an influence on the behaviour of the holes and the electrons in the plane perpendicular to the direction of the field. When the field is parallel to the growth direction of a quantum well structure, then the electrons are not spatially confined and the magnetic field has to overcome only the Coulomb binding. The determined radius is the radius of the exciton in the plane of the quantum well. When the field is perpendicular to the growth direction, then the charge carriers are also spatially confined. The magnetic field has to overcome both confinements and the determined exciton radius gives now an impression of the thickness of the quantum well.

2.4 Exciton properties

The magneto-photoluminescence technique is used to obtain information about the electron and hole confinement in quantum structures. The confinement is not measured in a direct way, but by interpreting the measured PL signals. First of all, the measured energy depends on several factors, such as the material and the size of the quantum structure. The line width of the PL peak is an indication of the size variation in the quantum structure. For most applications the aim is to produce quantum dots with a small size variation, and so a narrow line width. The PL intensity can give information about the confinement. A very low PL signal can indicate that the structure is a type-II system, in which the electrons and holes are spatially separated. The change of the PL energy as a function of the magnetic field gives information about the exciton properties. The exciton mass and radius also depend on several factors, which should be understood to interpret the results, and are discussed in more detail below.

2.4.1 The exciton mass

The measured exciton mass is a relative effective mass, as given already in equation (2.6). The effective mass of holes and electrons in a material differs from the mass of free electrons and holes. This difference from the free electron mass is caused by the forces of the crystal structure on the electron and depends on the material. The influence of the crystal structure on the exciton mass results in the dependence of the mass on the curvature of the energy bands [1]. The valence band is split into two bands, with a different curvature. So, there are two types of holes, heavy and light holes. The

heavy holes are in the highest energy band with less curvature. The light holes are in the lower band, which is more curved. For recombination, only the holes at the top of the valence band, the Γ-point, are important in our case. The concentration of light and heavy holes influences the measured exciton mass and mostly these concentrations are not equal. However, in general it is supposed that there are only heavy holes and the light holes are neglected.

The mass of the electron in the conduction band also depends on the curvature of the energy band. The mass of the electron is different when it is in the Γ-, the L- or the X-band. The energy bands in a quantum structure can be different from the bulk situation, for instance strain can change the band curvature. High masses are measured in self-assembled quantum dots due to the strain in the structure [7].

It was already mentioned that the effective mass depends on the material. This can be important for QWs and QDs. In the case that one of the charge carriers is not confined in the QW, this means that the effective mass is different compared to the case where both charge carriers are in the QW. When the QW is very small, the electron wavefunction will spill over into the barriers. This can also influence the average exciton mass, because it is probable for the electron to be in the barrier with a different mass [1].

The effective mass depends on the material, especially on its crystal structure. In the case of an anistropic crystal structure, this means that the mass can also be anisotropic. So a measurement with the field perpendicular to the growth direction will give, in most cases, another mass than a measurement with the field in another direction.

2.4.2 The exciton radius and the energy shift

Both the exciton radius and the total energy shift give information about the confinement of the exciton. The energy shift is defined here as the difference between the PL energy at 50T and the energy in zero field:

$$\Delta E = E(50T) - E(0T). \tag{2.16}$$

The diamagnetic shift is the total energy difference in the parabolic part, so from zero field to the crossover field B_c. The energy shift depends inversely on the confinement of the structure. When the confinement is weak, the crossover to linear behaviour happens at lower field values. The slope of the linear part is higher for light excitons, so the energy shift is higher for weakly confined and light excitons. When the spatial confinement is very strong, then the magnetic confinement can't exceed this and there won't be a change from parabolic to linear behavior. In this case the measured energy shift is equal to the diamagnetic shift.

The exciton radius is determined from the crossover field or can be estimated from the diamagnetic shift by using equation (2.17) and supposing that the exciton mass is known

$$\left\langle \rho^2 \right\rangle = \frac{8\mu \Delta E_{CM}}{e^2 \Delta B^2}. \tag{2.17}$$

In the case that the exciton radius is measured in the direction of quantum confinement, it will be an indication of the size of the quantum structure. When the exciton radius is bigger than the size of the quantum structure, this can indicate that it is a type-II structure, but this is not the only possibility. A large exciton radius can also occur in a type-I system, and then indicates spill over of the exciton wavefunction into the barriers. When a quantum structure decreases in size, then also the radius of the confined excitons will decrease. However when a certain limit is reached, then the structure becomes too small to confine the exciton. The confinement energy becomes too high and the exciton can relax by spilling over into the barriers. The radius will now increase again. When the curve has only a parabolic part, then the diamagnetic shift is used to estimate the exciton radius.

3 Production process of GaAs/$Al_xGa_{1-x}As$ quantum dots

There are several different methods to produce nanostructures, of which chemical vapour phase epitaxy and molecular beam epitaxy (MBE) are the two most used techniques. The aim of these growth techniques is to control the production of the nanostructures up to one monolayer. Quantum wells can be produced by these epitaxial growth techniques, but also quantum wires and dots, using patterned substrates or self-assembly. Molecular beam epitaxy and self-assembly are explained in detail here, because these are used in the production process of the studied samples. The specific production procedure for the samples is described in the next part. Dr. A. Rastelli and Dr. O. G. Schmidt of The Max Planck Institut für Festköperschung in Stuttgart[6] have made all the samples that are used for this research.

3.1 Molecular Beam Epitaxy

Molecular beam epitaxy, or MBE, is a method to grow epitaxial heterostructures. Epitaxy means growing a crystal layer of one material on a crystal substrate of another material, in such a manner that the crystal orientation of the growing layer is the same as the substrate crystal orientation. MBE is a process that happens in ultrahigh vacuum, on a heated substrate. The material to grow the layer is delivered to the substrate by a molecular beam, which is produced by evaporating molecules from solid-state sources in heated cells with an orifice directed to the sample surface.

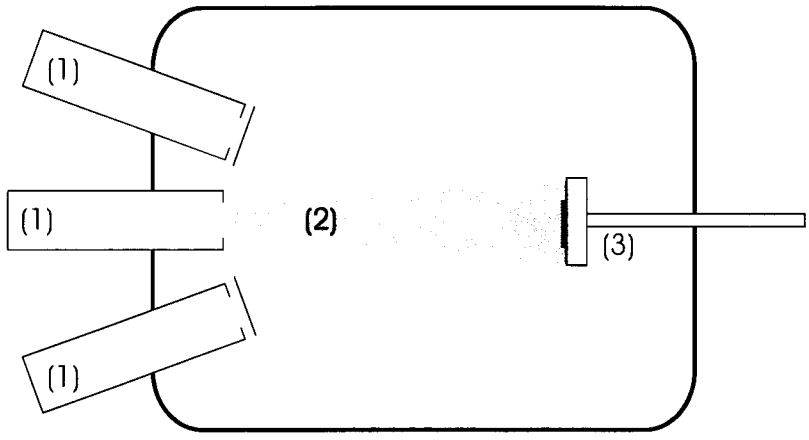

Figure 5: A schematic picture of a MBE-chamber with the Knudsen cells (1), the molecular beam (2) and the heated sample on the rotating holder (3).

In high vacuum, the mean free path of the molecules is larger than the width of the vacuum chamber, which means that the molecules can travel in straight lines to the surface without collisions. This

situation is called the molecular-flow regime or Knudsen regime of a gas and therefore the heated cells are called Knudsen cells. There are several Knudsen cells with different materials in an MBE, which can be opened or closed, to control the composition of the deposited layers. Another factor to control the deposition of the material is the substrate temperature. The substrate is annealed during the deposition of a layer in order that defects can be removed. However, when the temperature is too high, then unwanted diffusion will occur and blur the interfaces [1].

3.2 Self-assembly

When the epitaxially grown materials have the same lattice constant as the substrate, then the deposited materials grow into complete layers, one monolayer after the other, which is called the Frank-van der Merwe growth mode. It is also possible to grow a material on a substrate with a different lattice constant, such that the two materials are lattice mismatched. The deposited material won't form complete layers, but will grow in another growth mode, which is mostly the Stranski-Krastanow growth mode. In this growth mode self-assembled islands are formed on top of a wetting layer, which is used to make quantum dots by MBE.

The growth of self-assembled quantum dots in the Stranski-Krastonow mode is a two-step process. First, a one monolayer thick wetting layer is formed. The material of the monolayer is forced into the lattice constant of the substrate, which is different from its own lattice constant. The difference in lattice constant causes strain in the top material. When more material is put onto the wetting layer, the strain in the material is relaxed by forming islands instead of complete layers. When more material is deposited on the substrate, then the density of uniform formed dots increases or the dot size increases.

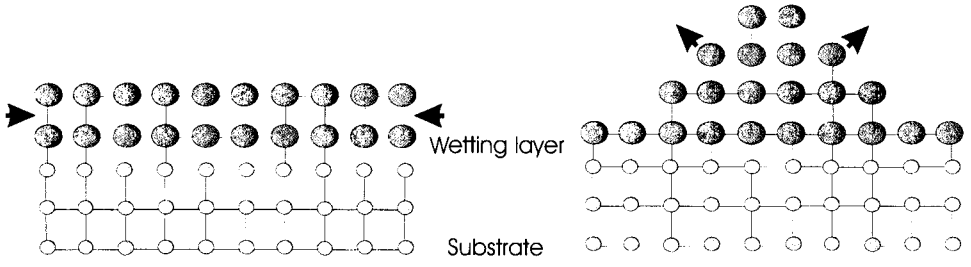

Figure 6: Self-assembled islands are formed on top of the wetting layer to relax the strain due to the lattice-mismatch between the substrate material and the deposited material.

The self-assembled dots are mostly capped by the same material as the substrate. Now there is strain in this capped layer at the places around the dots, because the top material is forced into the lattice of the dot material.

It is also possible that islands are formed directly on the substrate, without the formation of a wetting layer, which is called the Volmer-Weber growth mode. This one is not further discussed here, because the Stranski – Karastanow mode has found to dominate in the strained layer growth and is also applied in the production of the studied samples [11].

3.3 $GaAs/Al_xGa_{1-x}As$ quantum dots

AlAs (lattice constant a = 0.5660 nm) and GaAs (a = 0.5653 nm) are almost perfectly lattice matched, so when these two materials are growth on each other complete layers are formed, according to the Frank-van der Merwe growth mode. So, self-assembled quantum dots can't be made with these materials, but 'natural dots' can form in a $GaAs/Al_xGa_{1-x}As$ QW [12]. These natural dots are local increases of the well width of e.g. one monolayer, which cause a change in confinement energy and are sufficient to attract electrons and/or holes. The dots formed in this way vary a lot in size, which makes them less interesting. Another way of making $GaAs/Al_xGa_{1-x}As$ dots is making first a GaAs QW and then etching this QW. The disadvantage of etching is the rough interfaces with surfaces states, which influences the optical properties of the structure. Several other methods are demonstrated yet to make unstrained GaAs QDs such as cleaved-edge overgrowth and strain-induced confinement [13, 14]. In this method, a stressor, e.g. a self-assembled island, is deposited on top of the QW to induce strain in the well. The strain will change the energy bands at the specific places and so causes confinement. It is also possible to make a patterned AlGaAs substrate by etching and then filling up the etched holes with GaAs to obtain GaAs QDs [15].

The method that is used by Rastelli *et al.* to make $GaAs/Al_xGa_{1-x}As$ QDs is similar to this last method and combines self-assembly and etching, so the produced dots are self-assembled in an indirect way. The samples are produced with MBE, starting from a GaAs substrate. The production process is a single stage process, consisting of seven different steps, which are illustrated in Figure 7.

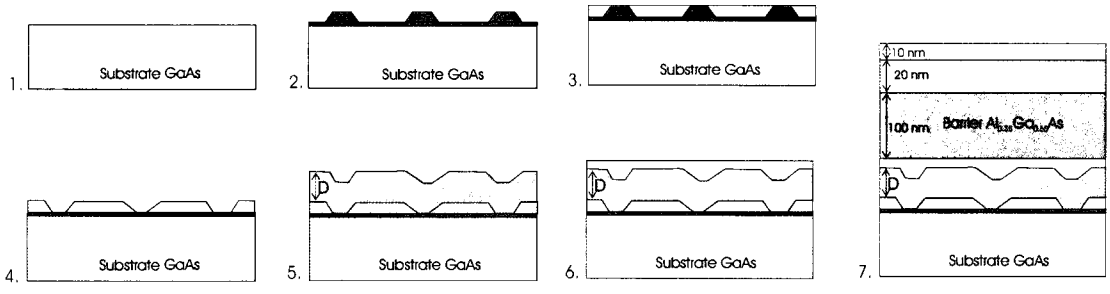

Figure 7: The production steps of the sample. The samples are grown by MBE, using a combination of self-assembly and etching.

InAs is deposited on a GaAs buffer layer in the first step. Because these two materials are lattice-mismatched, self-assembled InAs islands will form on top of an InAs wetting layer (1). The large InAs islands with a small size distribution are grown at a rate of 0.01 ML/s and a substrate temperature of 500° C. These InAs islands are overgrown with 10 nm GaAs (3) and then in situ etched by $AsBr_3$ gas for 5 nm (4). Strain-enhanced etching results in the preferential removal of the buried InAs dots and in this way nanoholes or antidots are formed at the place of the dots [16, 17]. Subsequently, an $Al_{0.45}Ga_{0.55}As$ layer with thickness D is deposited (5) on this GaAs surface with antidots. The thickness D of this layer is varied from 5, 7 and 10 to 15 nm. The antidots will be preserved at the $Al_{0.45}Ga_{0.55}As$ surface because of the low surface diffusitivity of Al at 500° C. The size of the antidots depends on the thickness D of the $Al_{0.45}Ga_{0.55}As$ layer. The next step is to fill the nanoholes with GaAs in order to make GaAs quantum dots (6). The antidots are overgrown with a nominally 2 nm thick GaAs layer. So, on top of the quantum dots, there is a GaAs quantum well. The thickness of the quantum well depends on the size of the dots (because there is always the same amount of material deposited). A 100 nm thick $Al_{0.35}Ga_{0.65}As$ barrier is grown on top of the quantum well (7). Notice that the two AlGaAs barriers have a different Al-concentration. The structure is completed with an $Al_{0.45}Ga_{0.55}As$ cladding layer of 20 nm and a 10 nm thick cap.

For this research five different samples are used with varying thickness D of the $Al_{0.45}Ga_{0.55}As$ barrier. One of the samples is a reference sample, which means that it consists only of a GaAs QW. In fact the steps 2 to 4 didn't occur in the production process of the reference sample. An overview of the sample numbers with the corresponding barrier thickness is given in Table 1.

Table 1: Five different samples are studied with varying barrier thickness D. Also the thickness of the wells and the dots are tabulated. The QD thickness includes the QW thickness, under which they sit. Sample 38 is the reference QW, without dots.

Sample number	**33**	**31**	**26**	**24**	**38**
D (nm)	5	7	10	15	7
QW thickness (nm)	1.70	1.76	1.82	1.86	2
QD thickness (nm)	6.30	5.76	5.32	4.36	-

As mentioned already, the depth of the antidots and so the thickness of the dots depends inversely on the thickness of the lower $Al_xGa_{1-x}As$, as illustrated in Figure 8. Rastelli *et al.*[6] measured the antidot size before filling with GaAs by atomic force microscopy (AFM) and scanning tunnelling microscopy (STM). The lateral size depends less on *D* than the antidot depth, and changes only in the $[1\,\bar{1}\,0]$ direction.

The antidots, and so the dots, have in general a flat, triangular cross-section, as illustrated in the right part of Figure 8. The total thickness is the antidot depth plus the thickness of the QW above. This thickness of the QW also depends on *D*, because always the same amount of GaAs is used to make the QDs and the QW. The QW thickness can be estimated from the total amount of GaAs, subtracting the part that is used to fill the antidots

$$d_{QW} \simeq d - {}^{V_{holes}}\!/_{u} \,. \tag{3.1}$$

When there are 30 holes per 1μm^2 and there is GaAs used to make a layer of d = 2 nm, then the thickness of the QWs and the QDs can be calculated and these values are also given in Table 1. Notice that the thickness of the well increases with increasing *D* and the thickness of the dots decreases.

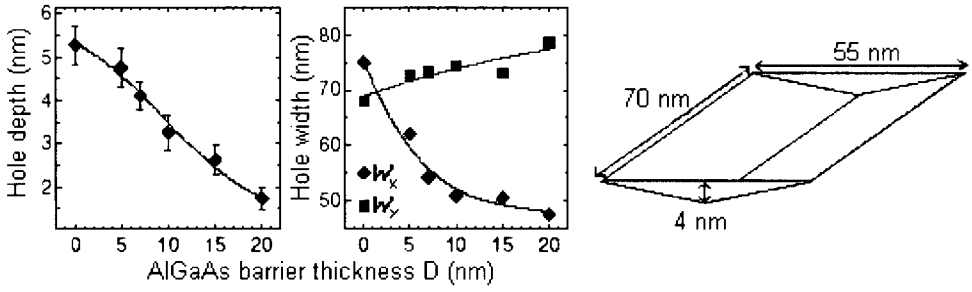

Figure 8: The dependence of the dot size on D is illustrated here. The two graphs at the left are data from Rastelli et al. The antidot depth and widths are measured with AFM and STM before the antidots are filled with GaAs (see production procedure). The dots have a flat, triangular cross-section as illustrated right [6].

3.4 The band structure and the Al-concentration

Both materials, GaAs and $Al_xGa_{1-x}As$, are studied a lot and the properties are well known, so a band diagram can be drawn for the studied structure by using the information from the literature [18, 19, 20]. Such a band diagram is useful for the later interpretation of the measurements, because it gives a first idea about the confinement of the electrons and the holes.

When the minimum in the conduction band is at the same k-value as the top of the valence band, the Γ-point, then the semiconductor is called direct. This means that for a recombination of an electron and a hole, only a radiative interaction is necessary. GaAs is a direct semiconductor, but AlAs is an indirect semiconductor. $Al_xGa_{1-x}As$ changes from a direct to an indirect semiconductor. This crossover happens at x = 0.4-0.45 [18]. The barriers of the structure studied here are asymmetric with one direct barrier and one indirect barrier. When the barrier is indirect, then the X-band is the lowest band, which is important for knowing the barrier height of the potential well. The asymmetry of the barriers can be

important in the case that the barriers are not high or that the wavefunction spills over in the barriers. The theoretical values that are used to draw the band diagram are from Vurgaftman *et al.* [19]. The band gaps for $Al_xGa_{1-x}As$ are calculated using

$$E_g\left(Al_xGa_{1-x}As\right)=(1-x)E_g\left(GaAs\right)+xE_g\left(AlAs\right)+x(1-x)C\,. \tag{3.2}$$

C is a bowing parameter in this equation, which changes for the different energy bands. The valence band offset changes linearly with x:

$$\Delta E_v = x\ 0.53\,eV \tag{3.3}$$

In this equation is 0.53 eV the valence band offset of GaAs/AlAs, and the error on this offset value is 0.05 eV [21, 22]. The calculated energy bands are for bulk material. In the case of a quantum structure, these values are the minimum energies, because the electron energy increases with the confinement energy, given in equation (2.4). An overview of the band diagram is given in Figure 9. The barriers in the conduction and the valence bands are quite high, 290 meV and 185 meV respectively, and so we can expect good confinement for both the charge carriers.

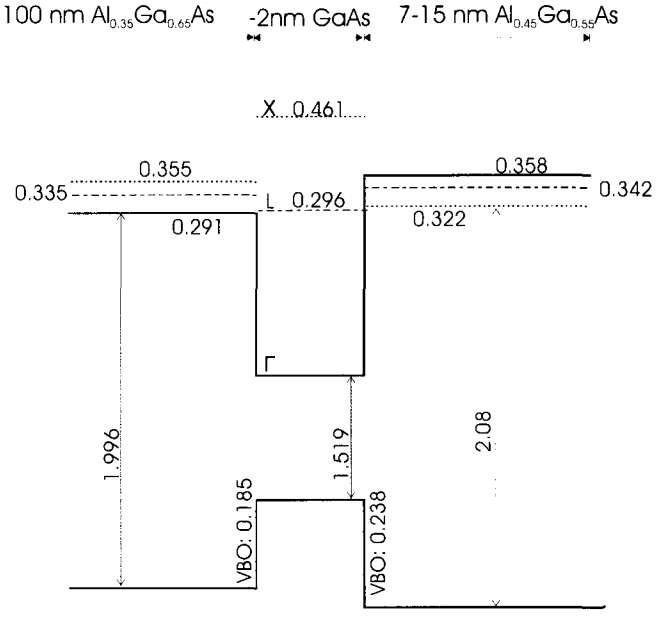

Figure 9: The band diagram of the GaAs/$Al_xGa_{1-x}As$ quantum well. All the numbers are in eV. In the conduction band the numbers at each band indicate the energy difference between that band and the Γ-band in GaAs. Notice that the right barrier has a higher Al-concentration, which makes this barrier indirect. The X-band is the lowest band at this side, but this band is still higher than the Γ- band in the left barrier. The valence band offset (VBO) is indicate at the transitions in the valence band.

4 The magneto-photoluminescence set-up

The aim of our magneto-photoluminescence experiments is to obtain information about the exciton confinement and the exciton properties, the mass and the radius. This information is obtained from the crossover from spatial to magnetic confinement, and the condition in equation (2.15) gives an idea about the magnetic fields that are needed to achieve this. Suppose that the exciton is confined in a dot with a radius of 5 nm, then the magnetic confinement exceeds the spatial confinement at a field of 52 T. This means that very high fields are needed for these experiments, which can be obtained by using pulsed fields. Working with pulsed fields implies that the measurement time is very short and that the timing between the optical set-up and the pulsed field set-up is very important [7].

4.1 The pulsed field laboratory

To produce fields up to 50 T special coils are developed and a capacitor bank to build up high voltages is needed. The capacitor bank in the laboratory can be connected to four high voltage coils in four different experimental set-ups, which can be used pseudo-simultaneously. The generation of high voltages and currents in the experimental set-up also requires a control of the safety of all the users and therefore the whole pulsed field lab is controlled by one central computer, 'the bank controller' [23].

To make constant fields up to 20 T super-conducting coils can be used, but when larger fields are advisable then the change from constant to pulsed fields is a 'cheap' option. There exist resistive DC magnets used to make fields up to 33 T e.g. in Nijmegen, but such an infrastructure is more expensive and consumes orders of magnitude more energy. The change to pulsed fields implies that the used coils are not superconducting and for these high field experiments special coils are developed and produced in the laboratory. Very high currents (up to 25 kA) are sent through the coil to generate the fields, which cause heating and large Lorentz forces acting on the wires. These forces make the internal reinforcement of the coil essential, which is done by covering each wire layer by a glass-fibre composite layer. Externally the magnet is reinforced by a stainless steel cylinder with carbon-fibre composite wound around it. This makes the coils very stable and they can withstand an average of about 1000 high field shots. A typical cross-section of such a coil is drawn in Figure 10. In spite of the internal and external reinforcement, the large heating of the wires will cause deformation of the coil, which influences the inductance. So measuring the inductance L gives information on the wear of the coil. Both the inductance L and the resistance R are measured continuously between the pulses to control the condition of the coil. The resistance R is used for monitoring the temperature of the coil. To reduce the heating of the coil the pulses are short, only 20 ms, and the coil is cooled with liquid nitrogen. After each pulse the coil has to cool down until the resistance has reached its low-temperature before another pulse is allowed to be maked [7, 23].

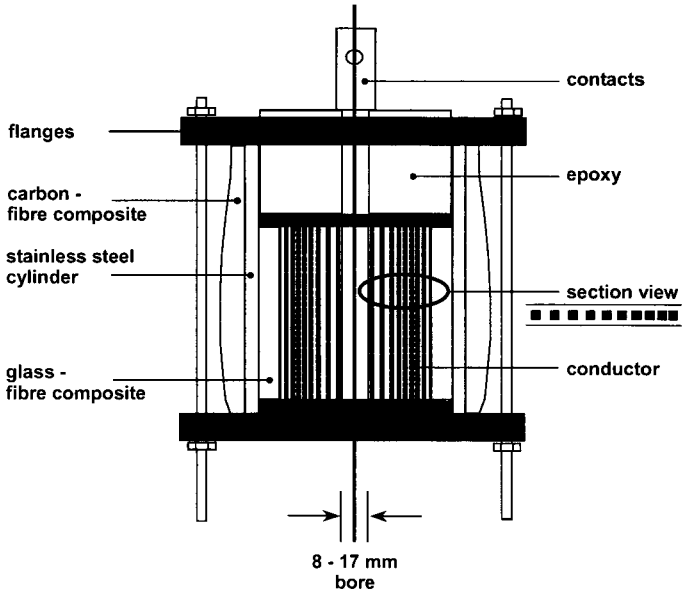

Figure 10: The cross-section of a typical coil. The coil is reinforced by covering each wire layer by a glass fibre composite layer. The coil is surrounded by a stainless steel cylinder and a carbon-fibre composite.

The second essential part of the pulsed field laboratory is the capacitor bank to build up the high voltages, which are discharged across the coil to make the high magnetic field. The laboratory has a 5 kV capacitor bank with a changeable capacity up to 40 mF and a maximum energy of 600 kJ. In this research the bank is always used at a capacity of 28 mF. The capacitor bank is loaded by a charge unit to a user-set voltage between 200 and 5000 V. When the required voltage is reached, the charge unit is disconnected. In case of emergency it is possible to discharge the bank quickly across a 100 Ω resistor. A slow controlled discharge across a 1 kΩ resistor is also possible. The normal discharging of the bank over the coil is controlled by four electronic thyristors, but there is also a mechanical switch, which is used during tests. Because the bank together with the coil and the wiring forms an LRC-circuit, the voltage on the bank will oscillate. A crowbar consisting of a 0.08 Ω resistance in series with a diode is added to this circuit to suppress oscillations. The diode also stops high reverse voltages on the bank and so spares the unipolar capacitors. A schematic drawing of the capacitor bank is given in Figure 11.

As already mentioned, four coils can be connected in parallel to the bank, allowing the performance of different experiments side by side. One coil at the time can be connected either to the bank for discharge, or to the LR sensor to measure the coil conditions. However during the cooling-down of one coil, which can take 40 minutes, another coil can be selected. This total set-up of the capacitor bank with the four coils is controlled by the central computer, which also used for the registration of magnetic fields, which are measured by a pick-up coil in the centre of the magnet. By measuring the

induced voltage as function of time the magnetic field can be calculated by integrating the Faraday's law, where S is the area of the pick-up coil [23]:

$$V_{pick-up}(t) = -S\frac{dB(t)}{dt} \tag{4.1}$$

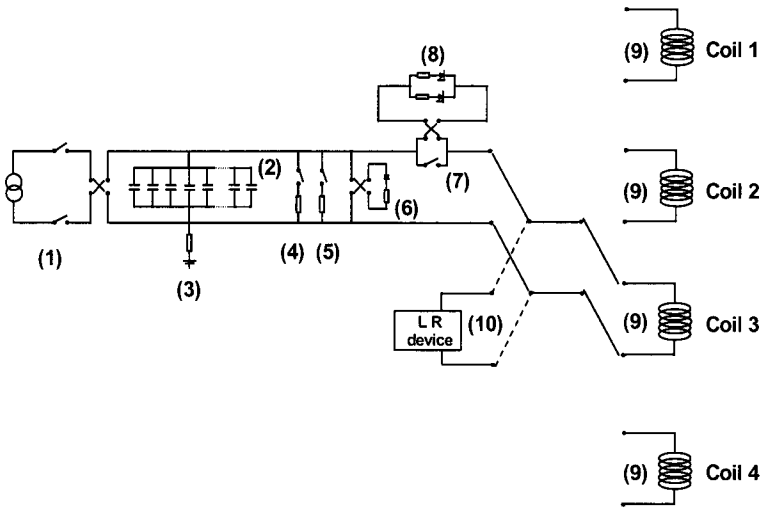

Figure 11: Schematic diagram of the 5kV capacitor bank: The charge unit (1) loads the bank (2). The bank can be discharged fast across a 100 Ω resistance (4) or slowly across a 1 kΩ resistance (5). The crowbar diode (6) suppresses oscillation in the circuit. The discharging of the bank across the coils is controlled by thyristors (8), but there is also a mechanical switch (7). Four different coils (9) can be connected to the bank and the L and R-values can be measured (10).

4.2 The photoluminescence set-up

The second part of the experimental set-up is the optical part, which consists of a Argon-ion laser and a spectrometer with a detector. The data measured by the detector are read out and stored by a computer. The Ar-ion laser has a changeable wavelength, but for these experiments it is used at the 514 nm line. The laser has a maximal output power of 15 W, but 500 mW is the maximum power used in the experiments because higher powers may damage the glass fibres that transmit the light to the sample. The luminescence light that comes of the sample is transmitted to the detection system that consists of a spectrometer connected to Image-intensified Charge Coupled Device or I-CCD. The spectrometer has a changeable resolution with three possible gratings: 1800, 600 or 150 grooves/mm. The selection of the gratings and the wavelength range is fully controlled by the optics computer and is fixed during one magnetic field pulse. For these experiments, mostly the grating with 600 grooves/mm is used and the slit size is between 70 μm and 520 μm. This gives a resolution between 0.42 and 3 nm, depending on the slit size. After the splitting of the light by the spectrometer,

it is detected by the I-CCD, which is sensitive from 400 to 850 nm. By quickly turning the intensifier on and off, it is used as an electronic shutter with speeds up to 10 ns. The detector can measure three spectra before the data have to be read out by the computer. This is possible by using only one third of the array of 576x384 pixels for each spectrum. The smallest size of the CCD is used for the wavelength range. In the long direction the CCD is covered for two thirds, such that for each measured spectrum an array of 192x384 pixels is used. After the first illumination of the CCD, the photo-induced charge collected by the first 192 lines is moved to the next 192 lines in the middle of the array. The first part of the CCD is now again unloaded for the second exposure. In this way it is possible to measure three spectra during a pulse of only 20 ms at three different field values. There has to be at least 0.3 ms between two exposures to allow the CCD to shift the collected charges down[8]. Each measurement takes only 0.5 ms, so that the field variation during the measurement is less than 3%. The field varies slower at the maximum field of the pulse, with only 0.5%. For samples with a low luminescence intensity one measurement of 4 ms, with also only 5% field variation, can be done during one pulse.

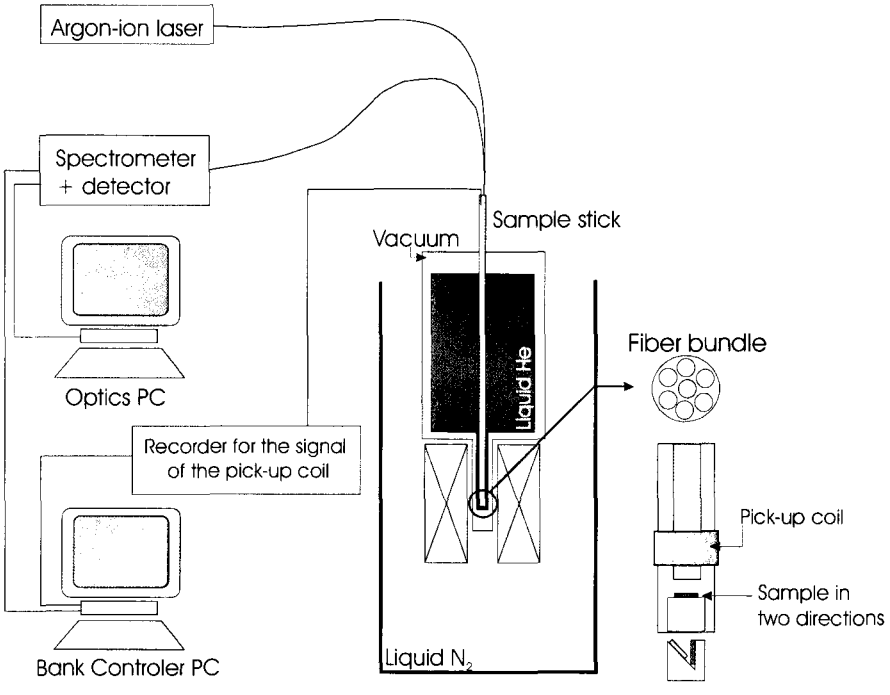

Figure 12: An overview of the cryostat with the photoluminescence set-up. The pick-up coil is used to measure the magnetic field and to generate a trigger signal for the optical measurement. An optical fibre bundle is used to transmit the light to and from the sample. The sample can be mounted in the magnet in the horizontal and vertical direction, where in the vertical case a mirror is used to reflect the light to and from the sample.

The studied sample is placed in the core of the magnet for the magneto-photoluminescence measurements, which implies that the laser light and the luminescence light has to be transmitted

between the sample and optics set-up. This is done by a glass fibre bundle of seven fibres with a core of 200 μm. One fibre is used for the transmission of the laser light and the other six fibres are used for the collection of the luminescence light that comes of the sample. The sample can be placed in the magnet in two directions: horizontally with the field perpendicular to the sample surface or vertically with the field parallel to the surface. When the sample is mounted vertically, then a mirror is used to reflect the light on to the sample.

The luminescence process is dependent on temperature, which is kept constant by immersing the sample in liquid helium at 4.2 K. In this way the heating by the laser light is restricted as much as possible. A cryostat is used to isolate the helium-cooled sample from the liquid nitrogen, which cools the magnet. The cryostat consists of two concentric tubes, which are mounted in the centre of the coil. The sample is mounted in the central tube, which is filled with liquid helium, while the space between the two tubes is pumped vacuum for isolation. An overview of the cryostat with the optical set-up is given in Figure 12.

The timing between the generation of the magnetic field and the registration of the optical signal is an important point in these experiments, and is also controlled by the bank controller PC. It is the pick-up coil, used for the measuring of the magnetic field, which gives a trigger signal for the optical timing that goes via the bank controller to the optics PC. During the magnetic field pulse, several spectra can be taken at specific field values by using pre-programmed shutter openings. To have a good timing between the shutter openings and the field pulse, the start of the shutter sequences is given by the large change of voltage over the pick-up coil at the start of each pulse.

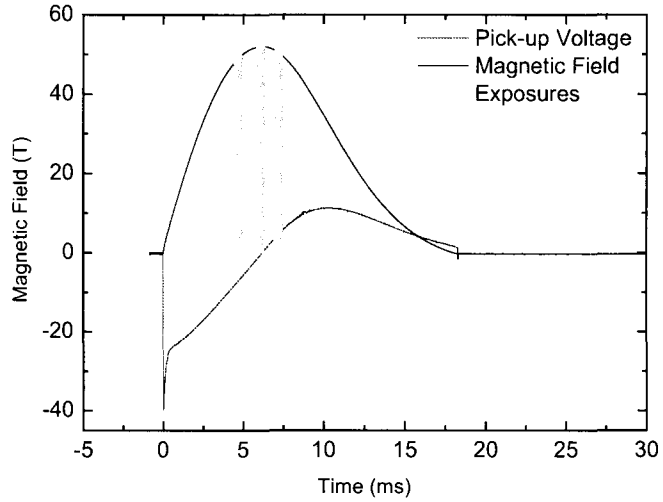

Figure 13: A typical field pulse profile with the pick-up voltage. The sharp spike in the pick-up signal is used as the trigger signal. The grey bars indicate the three shutter openings of the detector.

5 Results and discussion

The magneto-photoluminescence technique is used to study the optical properties of the GaAs/$Al_xGa_{1-x}As$ quantum structure. The PL data are presented and discussed in this chapter, which is divided into two main parts. The first, biggest part is about magneto-photoluminescence of the quantum structure. The second part is about the dependence of the PL energy on the laser intensity. During the whole discussion a distinction is made between the measurements on the QDs and the QWs, which are compared with each other.

We start with a short discussion of the total PL spectrum of a sample, as shown in Figure 14. There are four peaks in this spectrum, starting with the PL peak of the InAs wetting layer at the lowest energy side. The next peak, at 1.49 eV, comes from the GaAs substrate. The two peaks at higher energy are the main interest of this work. The peak at 1.62 eV comes from the QDs and the 1.78 eV peak is the PL of the QW. The background at the higher energy side is probably due to the $Al_xGa_{1-x}As$ barriers.

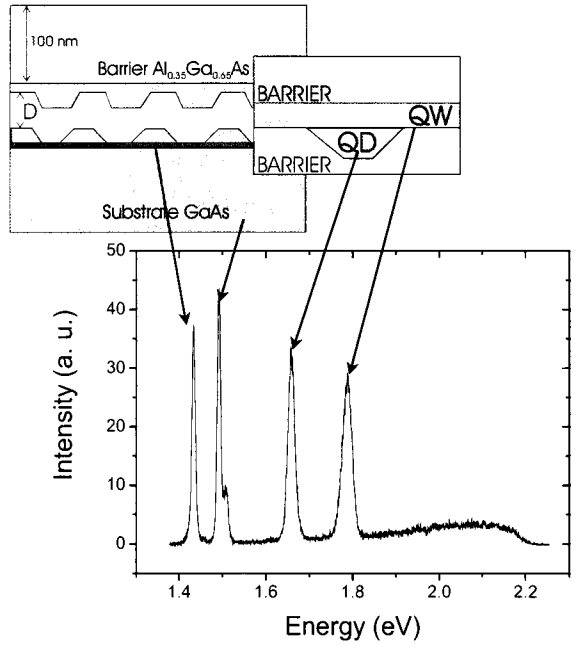

Figure 14: The spectrum of sample 26 with, from left to right, the PL peaks of InAs wetting layer, the GaAs substrate, the QDs and the QW. The background at the higher energy side is probably caused by the $Al_xGa_{1-x}As$ barriers.

Notice that the PL energy of the GaAs substrate is lower than expected for pure bulk GaAs, which has a band gap of 1.52 eV. This energy difference is possibly due to impurities in the substrate, *e.g.* carbon acceptors, which lower the photoluminescence energy.

The presented spectrum is a general spectrum for the samples with a QW and QDs, *i.e.* samples 24, 26 and 31. The reference sample 38 has only a QW, so there are only two peaks in its spectrum. Also sample 33 has a spectrum with only three peaks, but now the QW peak is missing. The signal of the QW is too weak to measure in this case. This means that there are four QD PL peaks and four QW PL peaks to study.

5.1 Magneto-photoluminescence

The magneto-photoluminescence data, discussed in this section, are the biggest part of the research. These measurements give information about the exciton radius and mass, as explained before, and are therefore useful to understand the optical properties of the QWs and the dots. The discussion starts with the QWs.

5.1.1 The quantum well

The QW in this type of structure is analogous to a wetting layer in the case of real self-assembled dots. Just as with a wetting layer, these QWs are very thin with a maximum thickness of 2 nm or about 7 monolayers (ML), where one ML is 0.28 nm. This implies that the confinement energies of the electrons will be high.

5.1.1.1 The magnetic field parallel to the growth direction

A magnetic field influences the electrons in the directions perpendicular to the field, which for B parallel to the growth direction z (B//z) means the plane of the QWs. The measured masses and radii are thus the in-plane values. The PL energy as function of B is plotted in Figure 15 for the four samples and the results that can be derived from these data are given in Table 2. Several different things can be said about these data. First of all, the PL energies are different in zero field for the four samples. There is a clear gap of 17 meV between the PL energy of sample 31 and the three other samples. This PL energy difference between the samples is caused by the difference in thickness and in roughness (of the interface) of the QW. The QW thicknesses of the sample 38, 26 and 24 are all around 7 ML as given in Table 2, while sample 31 has the thinnest quantum well of only 1.76 nm or almost 6 ML. This discrete change in thickness explains the big energy difference between this sample 31 and the other three samples. The PL energies of QWs 26 and 24 are a bit higher than in the case of the reference QW, due to a difference in roughness. The QW thicknesses are between 7 and 6 MLs thick, which make their interface rougher and increase their PL energy in comparison with the reference QW.

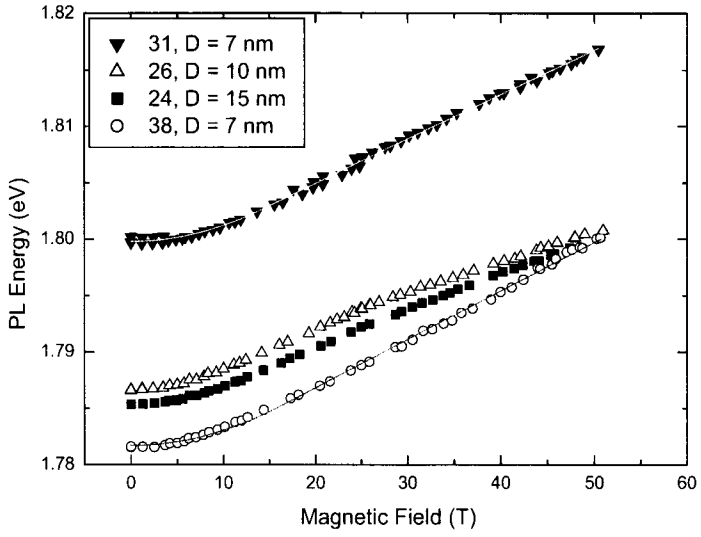

Figure 15: The centre of mass of the QW PL peak as function of the magnetic field. The energy dissimilarity at zero field is due to the difference in thickness between the wells. The exciton mass is calculated from the slope of the linear parts of the curves.

The four curves all have a parabolic behaviour at low field, which changes to a linear behaviour in high fields. However, graph 26 shows a varying slope, with a kink around 30 T. Also graph 24 deviates a bit from a linear behaviour, but not so clearly as sample 26. The mass is derived from the slope and therefore two mass values can be calculated for sample 26. The masses are given in Table 2 and discussed in more detail in the next paragraph.

Table 2: Overview of the PL data on the QWs with B//z. The exciton radius of sample 26 is calculated from the first part of the graph. Notice that the measured exciton masses are high in comparison to the mass in bulk GaAs. The energy shift is higher for the samples 38 and 31. The line width is also given in the table, which is smaller for sample 31.

Sample nr.	**D (nm)**	**E_{CM} (eV ± 0.0005 eV) at $B = 0T$**	**ΔE_{CM} (meV ± 0.5 meV)**	**Line width (meV ± 0.5 meV)**	**Reduced mass (m_e ± 0.01 m_e)**	**Exciton radius (nm ± 0.2 nm)**	**QW thickness (nm)**	**Number of MLs**
38 Reference	7	1.781	18	10-11	0.13	8.9	2	7.1
31	7	1.80	17	7.5-8.5	0.15	9.8	1.76	6.2
26	10	1.785	7.5 6.5	10-11	*0.16* *0.21*	11.6	1.82	6.5
24	15	1.796	14	10-11	0.17	11.7	1.86	6.6

- *The mass*

Comparing the measured masses in Table 2 with the theoretical masses in Table 3, it is clear that the measured masses are all more than twice the value for an exciton in the Γ-band of GaAs. These high masses can be explained by the non-parabolicity of the conduction band in very thin QWs [24].

Table 3: Theoretical reduced exciton mass in bulk material for the Γ-, L- and X-band [19]. For the calculation of the exciton masses in the barriers, it is supposed that the holes are always well confined in the GaAs QW. The masses are different in the two $Al_xGa_{1-x}As$ barriers because of the different Al-concentration.

	Γ	L	X
GaAs	0.056	0.15	0.217
$Al_{0.35}Ga_{0.65}As$ Upper barrier	0.075	0.15	0.206
$Al_{0.45}Ga_{0.55}As$ Lower barrier	0.22	0.22	0.22

The confinement energy depends inversely on the mass of the charge carriers and the dimension of the structure, as explained in paragraph 2.1. This means that the energy levels shift up to higher values when the size of the quantum structure decreases and that light particles are more influenced by these decreasing dimensions. As a consequence, the electrons in the Γ-band, with a small mass, are more influenced by the changing thickness of the QW than electrons with a higher mass in the L- or the X-band. The difference between the bands decreases and the curvature of the Γ-band changes, which is seen as an increase of the mass. This effect becomes important in QWs thinner than 10 nm (for GaAs) and is illustrated in Figure 16.

The reference QW has the smallest mass, which is in agreement with this explanation, because this QW is the thickest one. However, the thinnest QW, of sample 31, should have the excitons with the highest mass, which is not the case. The exciton masses of samples 24 and 26 are both higher, which must have another reason than the thickness of the QWs. A lot of other factors also influence the mass, for instance the overlap of the wavefunction into the barriers and the proportion of light to heavy holes. This last factor probably can't explain the mass difference because this is likely to stay the same for all the samples. The wavefunction spill over is interesting to look at, because the barrier thickness D is different for these samples, so the penetration into the barriers is also different.

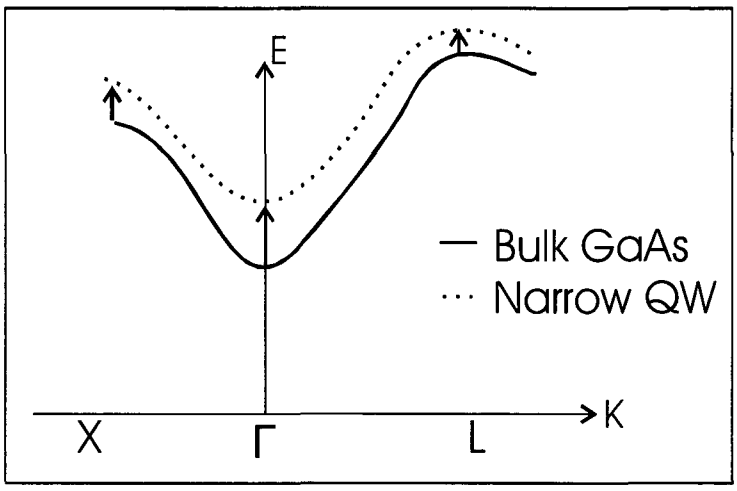

Figure 16: The non-parabolicity of the bands causes an unequal energy shift in a narrow QW. The curvature of the Γ-band changes, which results in an increase of the electron mass. This effects becomes important in quantum structures with sizes smaller than 10 nm.

The penetration of the exciton wavefunction into the barriers is mostly due to the electrons. The wavefunction of heavier holes is less influenced by the well thickness and moreover, the exciton mass is dominated by the lighter particle, *i.e.* the electron. Therefore the influence of the hole is not discussed here and the mass difference is totally explained by a changing electron mass. When the electron wavefunction moves into the barriers, this influences the properties of this electron because the effective electron mass depends on the material. When the electron can be in the barrier with a certain probability, the mass is then an average value of the two different mass values [1]. The effective mass in the lower barrier is clearly higher (Table 3), which causes an increases of the electron mass. Because the QWs are very thin, there is a lot of overlap and this factor can be important. Suppose now that the overlap into the barriers is almost the same for the four samples, but in the case of the thin barrier the wavefunction spills over into the substrate, which lowers the mass again.

The high mass values are explained now, but there is more going on in sample 26. For this sample the slope clearly decreases, which indicates an increase of the mass. The mass can change when the electron energy raises, so that the electron passes to a higher energy band with another mass. But also other factors, as the spin or the angular momentum, can influence the slope, which are not taken into account in the used model. In that case, the mass of sample 26 can't be calculated and its values in Table 2 are wrong. The energy difference between the lowest band, the Γ-band, and the next band is bigger than the total energy shift, so a crossover from one band to the other is not likely. This means that something else is going on and the mass can't be calculated. Notice also that this changing slope is not measured when the laser intensity is very low.

- *The photoluminescence line width*

We now discuss the PL line width as function of the field, as plotted in Figure 17, where two things have to be explained. The first thing is the difference in line width between the samples. Two factors have the main influence on the line width: the QW thickness and the interface roughness [25].

Suppose first that the excitons are well confined in a QW, without spill over of the wavefunctions. Then the degree of roughness influences the line width. The degree of roughness is higher when there are more and smaller thicker (or thinner) islands in the lateral direction of the QW. When a thicker island is big enough, then an exciton can relax in this island by increasing its vertical size and lowering its confinement energy. The excitons in the thinner part of the QW are more confined in the vertical direction and this results in a higher energy. These two different situations cause a broadening of the line width and are illustrated in the left part of Figure 18. This is the situation for sample 38, which has the highest line width.

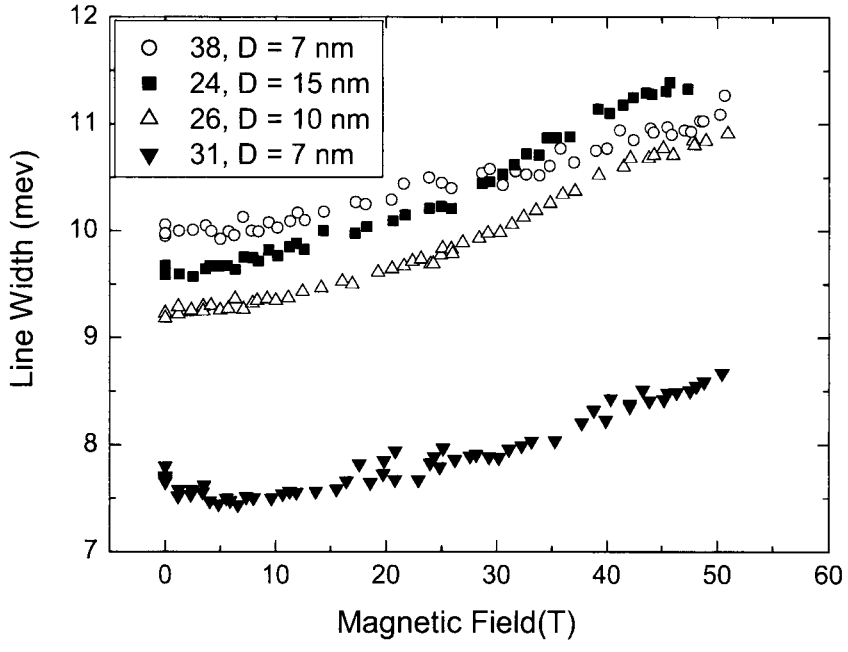

Figure 17: The line width as function of B, with B//z. There is a shift in line width between the samples with a 7 MLs thick QW and the sample with a 6 MLs thick QW. The line width increases as function of field.

Suppose now that the average thickness doesn't change, but that there are more, smaller islands. The exciton can't 'relax' in these small islands, so it can't lower its confinement energy. The variation in energy and in wavefunction size is lower in this situation, which is the case for the samples 26 and 24. These QWs have almost the same thickness as QW 38 but the interfaces are rougher.

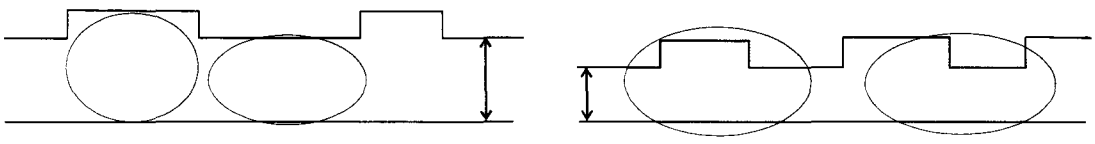

Figure 18: The exciton radius is influenced by the thickness and the roughness of the QW. The variations in the thickness of the QW causes variations in the confinement energy, certainly when the thicker islands are big enough. In the case of a very thin QW, the wavefunctions spills over into the barriers and is no longer sensitive for the roughness of the interface, as illustrated at the right. This effects in a decrease of the line width.

If the QW is very thin, than the exciton wavefunction will spill over into the barriers, which decreases the confinement. The exciton size is now less influenced by the interface roughness. This results in less size variations in the vertical direction, as illustrated in the right part of Figure 18. Sample 31 has the lowest line width and it is indeed the sample with the thinnest QW. The big shift between sample 31 and the other three samples is due to a discrete change in thickness from 6 to 7 ML (see Table 2) and is consistent with the big shift in PL energy between the samples (Figure 15).

A second thing to explain is the increase of the line width as function of field. The exciton wavefunction becomes narrower in field, so the exciton can fit into the narrower and thicker islands. This will again cause a relaxation of the wavefunction in the vertical direction and a narrowing in the lateral direction. The magnetic field makes the exciton more sensitive to the thickness variations of the QW as illustrated in Figure 19.

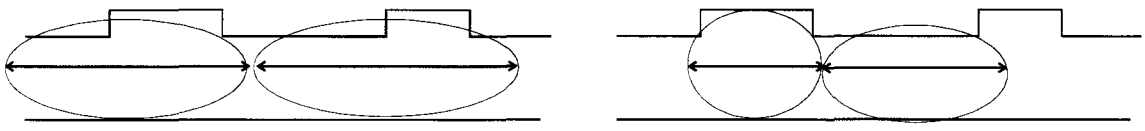

Figure 19: The line width is influenced by the magnetic field. The left picture is the case without field. The wavefunction is squeezed in a magnetic field as illustrated at the right. The wavefunction is now more influenced by the thickness variations.

5.1.1.2 *The magnetic field perpendicular to the growth direction*

Now the field direction is changed from $B//z$ to B perpendicular to the growth direction ($B \perp z$), to measure the confinement and the exciton properties in the growth direction. The PL data of the four QWs are plotted in Figure 20 and the results are summarized in Table 4.

The four curves don't show a crossover from a parabolic behaviour to a linear behaviour, which indicates that the spatial confinement is much stronger in this direction. This is also confirmed by the

small diamagnetic shift, around 3 meV for all the samples. Notice that the curves 24 and 26 are well fitted with a parabola, while the data of samples 31 and 38 are much more noisy. The signals of these last samples were much weaker, which probably explains the fluctuations on these data.

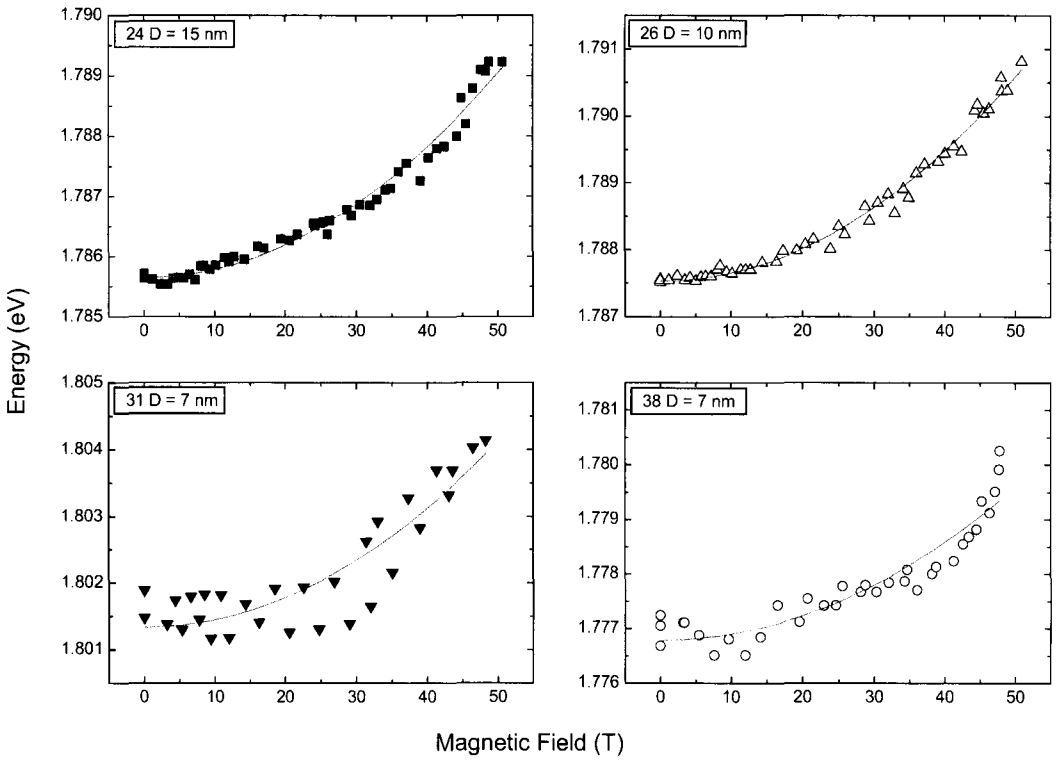

Figure 20: The PL energy as function of the magnetic field. Sample 26 has a clear parabolic dependence on the magnetic field. The diamagnetic shift is almost the same for all the samples.

The data without a linear part give no information about the exciton mass, but a minimum and a maximum value of the exciton radius can be estimated. The minimum value is estimated from the diamagnetic shift, using formula (2.17). The radius depends linearly on the exciton mass, which is not known for these measurements. The mass measured in the other field direction can't be used for this calculation because it is anisotropic. Supposing that the electron is in the Γ-band of GaAs, the value for bulk GaAs, $\mu = 0.056\ m_e$, is used. Since this mass is certainly smaller than the effective mass in a thin QW, the calculated radius is indeed a minimum value. The calculated radii are represented in Table 4 and the exciton diameter for all the samples is bigger than 3 nm. When the QW-thickness is maximum 2 nm, this means that the exciton wavefunction is too big to be completely in the QW, i.e. the exciton wavefunction spills over into the barriers in the z-direction.

A maximum value for the exciton radius of 5.13 nm is found supposing that the linear regime begins at the end of the graph at 50 T. These minima and maxima give a large range on the possible exciton radius. In general, it can be concluded that the excitons are weakly confined in the QWs.

Table 4: PL data on the QWs with B⊥z. The tabulated energy shift is in this case the diamagnetic shift between 0 and 50 T. The exciton radius is a minimum value estimated from the diamagnetic shift. From a comparison of these minimum radii with the QW thickness, it is concluded that the wavefunctions spill over into the barriers.

Sample nr.	D (nm)	E_{CM} (eV ± 0.0005 eV) at B = 0T	ΔE_{CM} (meV ± 0.5 meV)	Line width (meV ± 0.5 meV)	Minimum exciton radius (nm ± 0.2 nm)	QW thickness (nm)
38 Reference	7	1.777	3.6	17	1.9	2
31	7	1.801	2.7	11.5	1.6	1.76
26	10	1.787	3.3	9.5	1.8	1.82
24	15	1.785	3.5	9.5	1.9	1.86

The dependence of the PL intensity on the magnetic field can also give more information about the confinement and is therefore plotted in Figure 21. It is remarkable that the intensity behaviour of the samples 38 and 31 differs a lot from the intensity curves of samples 26 and 24.

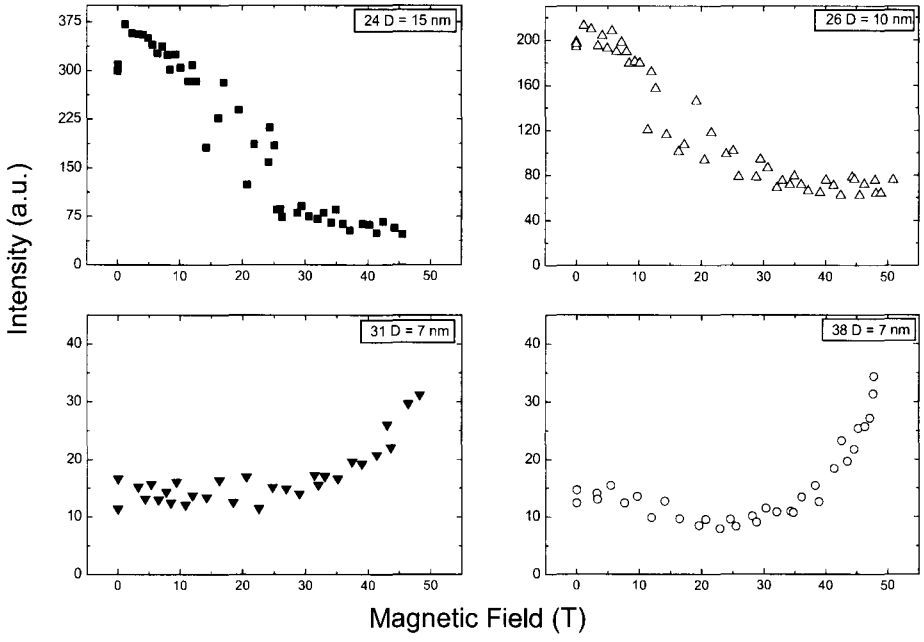

Figure 21: PL peak intensity as function of the magnetic field. The samples with a thin barrier have an increasing intensity and the samples with thick barrier have a decreasing intensity.

Initially the PL intensities of the samples 38 (Reference QW) and 31 are much lower, but they increase as function of the magnetic field. For the other two samples the opposite is true, the intensity is initially high and then decreases with field. Notice that at high fields the intensities of all the four samples are at almost the same value. Reasons for the intensity increase could be that the overlap between the electron and the hole wavefunctions increases or that more electrons stay into the QW in higher fields. A decrease of the intensity then indicates the opposite: a decreasing overlap of the wavefunctions or escaping electrons in higher fields. So, two different things are going on in the two pairs of samples.

Looking to the line width as function of B, which is plotted in Figure 22, again two types of behaviour can be distinguished. Sample 38 and 31 have a comparable behaviour that is different from the behaviour of the two other samples and in high fields the line width is almost the same for all the samples (except sample 31).

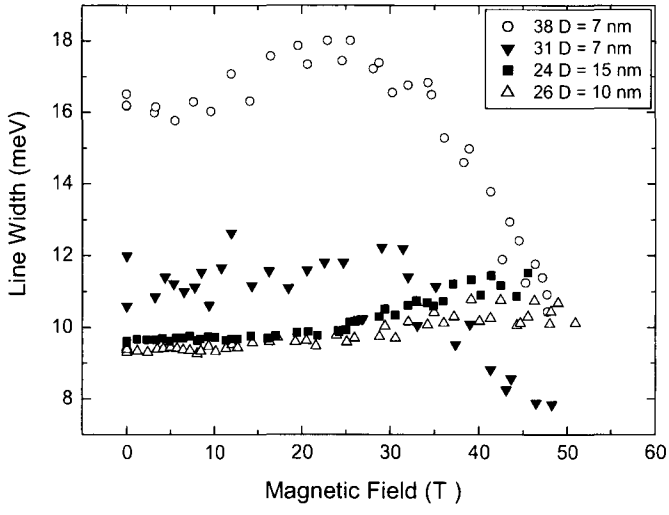

Figure 22: The line width as function of B for the different samples. The samples 26 and 24 have the lowest line width, which is almost constant. The line width of the two other samples is higher and with a large decrease in higher fields.

For the samples 26 and 24 the line width is constant up to 30 T and increases then a little bit. But for the other two samples the line width decreases a lot when the field increases above 30 T. It has been explained already for the other field direction that the magnetic field can cause an increase of the line width when the QW is very thin and the wavefunction spill over becomes important. But now the line width decreases in two cases while all the QWs are almost of the same thickness.

The line width of the peak of the reference quantum well is much higher than the others because this PL peak is asymmetric. The photoluminescence peak seems to exist of two peaks. When the magnetic field increases, then one peak seems to disappear. (When the magnetic field was in the z-direction,

then the QW-peak wasn't asymmetric, even not in zero field.) Also the line width of sample 31 is higher in low fields, while this peak is not asymmetric.

- *The barrier thickness*

We conclude from the intensity and the line width that there are two types of samples. Moreover, these two types of samples differ from each other by another factor, the lower barrier thickness *D*. The samples with an increasing intensity have a thin barrier, meaning 7 nm or less. The other samples, with a decreasing intensity, have a thicker barrier. This difference in barrier thickness causes the different behaviours.

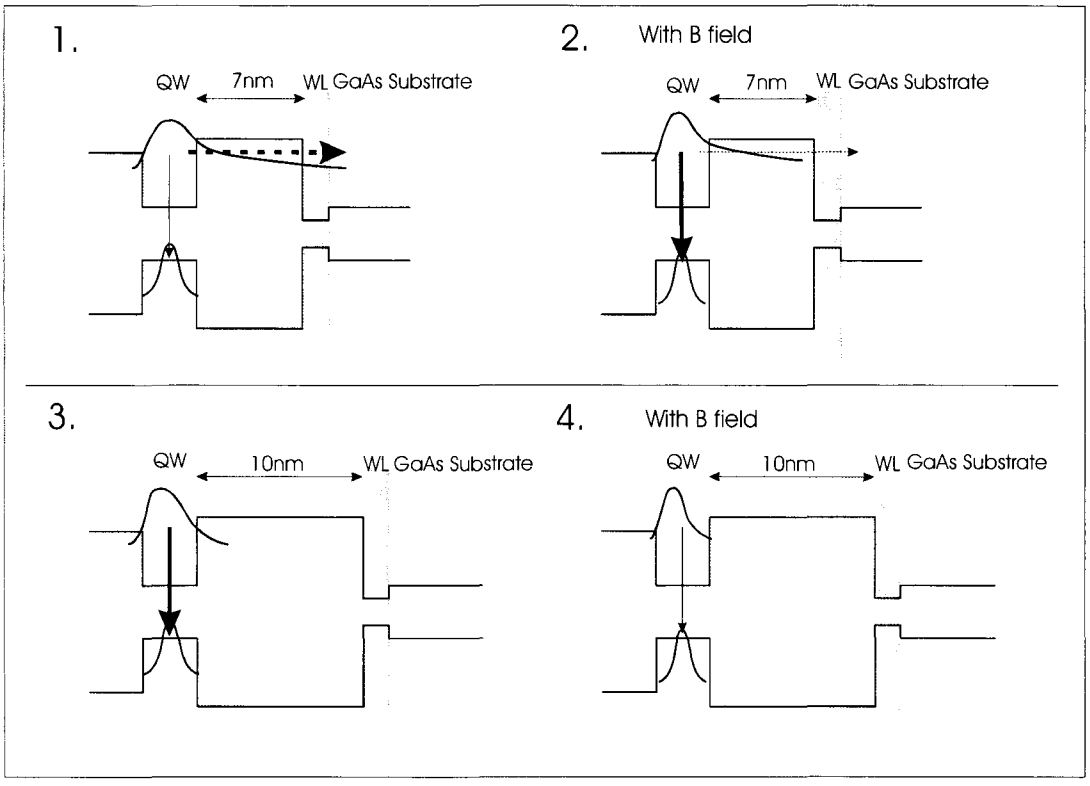

Figure 23: The tunnelling through a thin barrier with and without field is illustrated in the upper half of the figure (1, 2). The vertical arrow indicates the recombination, while the horizontal arrow indicated the tunnelling. The tunnelling is suppressed in field, which implies an increase of the recombination (2). In the lower half (3, 4) a sample with a thick barrier is illustrated. The electron and hole wavefunction are offset, which implies a decreasing overlap (4) in field and thus decreasing recombination intensity.

When the lower barrier is thin enough, then the QW and the GaAs substrate become coupled. We know from the estimated exciton radius that the electron wavefunction spills over into the barriers. This wavefunction spill over makes it possible for the electrons to tunnel from the QW through the thin barrier into the substrate, where they are in a lower energy state. This implies that there are less electrons recombining in the QW, which explains the lower intensity in zero field for the samples with a thin barrier. This also explains why there is no QW PL signal in the case of sample 33, as mentioned

in the beginning of this chapter. This sample has the thinnest barrier (only 5 nm), so most of the electrons tunnel out the QW before they recombine with a hole in the QW. When a magnetic field is applied, then the electron wavefunction is squeezed. The penetration of the wavefunction into the barrier decreases, thereby increasing the tunnelling time and so decreasing the tunnelling probability. So the magnetic field suppresses the tunnelling, *i.e.* more electrons stay in the QW and recombine there, which explains the PL intensity increases.

For the other type of samples the barrier is thicker, so the tunnelling time is bigger than the recombination time in the QW. This means that the electrons recombine with a hole before they can tunnel and the PL intensity is initially higher. The increase of B causes again the squeezing of the wavefunctions. The $Al_xGa_{1-x}As$ barriers are asymmetric, which causes an asymmetric wavefunction spill over for the electron wavefunction. The asymmetry of the electron wavefunction causes the electron and the hole wavefunction to be slightly offset. So, the squeezing of the wavefunctions in this case decreases the overlap between the wavefunctions, which explains the decreases of the PL intensity.

The difference between the two types of samples is illustrated in Figure 23. The tunnelling probability can be estimated by calculating the tunnelling rate through the barrier and comparing this with the recombination time in the QW. For a rough estimation the barrier is approximated by a square barrier.

5.1.2 The quantum dot

In this part the properties of the QDs are discussed, which are the main interest of this research. The same types of measurements are done on the QD PL peaks as on the QW PL peaks. Comparing the QD data with the results on the QWs will help understanding the properties of the dots. The discussion starts again with the measurements with B//z.

5.1.2.1 The magnetic field parallel to the growth direction

Just as for the QWs, the in-plane properties of the exciton are derived from these data. The difference with the QWs is that in this case the electrons are also limited in the lateral direction by the size of the dots. The dots have a triangular and flat shape, that depends on the barrier thickness D as illustrated in Figure 8. The thickness of the QW should be added to the hole depth to obtain the total dot thickness as given in Table 5. The widths of the dots given in Figure 8 are large in comparison with the measured exciton diameter (of ± 20 nm) in the wells, so from these numbers only no lateral confinement is expected. However, the dot shape is triangular and the lateral size decreases rapidly, which certainly influences the average exciton diameter. The exciton radii are calculated from the data, which are shown in Figure 24, and the values are given in Table 5. Indeed the excitons are smaller in the dots as in the wells, which indicates lateral confinement.

Table 5: The PL data on the QDs with B//z. The thickness and the widths of the dots are data from Rastelli et al.[6] The QD thickness is the deepness of the nanoholes plus the estimated thickness of the QW.

Sample nr.	D (nm)	E_{CM} (eV ± 0.0005 eV) at $B = 0T$	ΔE (meV ± 0.5 meV)	Reduced mass (m_e ± 0.01 m_e)	Exciton radius (nm ± 0.2 nm)	QD thickness (nm)	QD width (nm)
33	5	1.610	17	0.11	6.6	6.30	60-72
31	7	1.623	18.3	0.12	7.6	5.76	55-73
26	10	1.658	18.8	0.13	9.4	5.32	50-73
24	15	1.694	16.7	0.15	10.4	4.36	48-75

The exciton size varies more in the case of the dots, while the lateral size doesn't change a lot for the different samples (see Table 5). The reason for this changing size is the decreasing thickness of the dots. In the thicker dots the exciton wavefunction is broaden in the vertical direction, which lowers the exciton energy. At the same time, the lateral confinement increases and the energy in the lateral direction increases, but the vertical decrease of energy is the strongest effect.

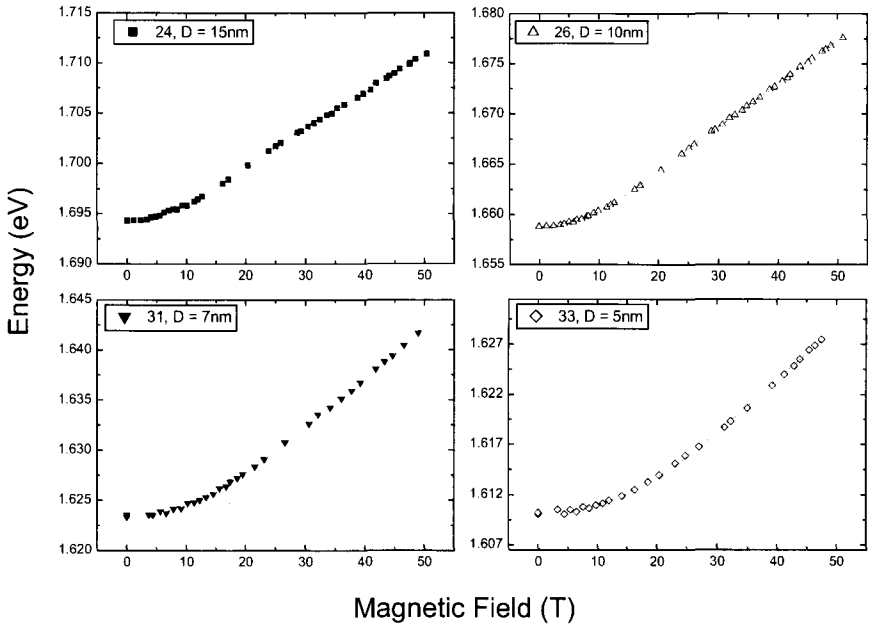

Figure 24: The PL-energy of the QDs as function of B, with B//z. The four curves all have a comparable energy shift.

In the case of a thin dot, then the vertical confinement is stronger, but the lateral confinement is weaker. So the wavefunction can broaden in the lateral direction as illustrated in Figure 25.

Comparing this with the wells, then the smaller exciton size in the dots is due to the lateral confinement, but also to the 'relaxation' of the wavefunction in the vertical direction.

Also the exciton masses are given in Table 5, and the dependence on the dot thickness is the same as for the wells. The mass is the smallest in the thickest dots (samples 33 and 31) and clearly smaller than in the wells. But for the thinner dots (samples 26 and 24) the masses are comparable with the values in the wells, even though the dots are thicker.

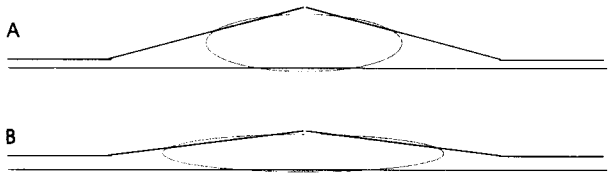

Figure 25: The exciton energy lowers in a thick dot (a) because of the lower vertical confinement. At the same time the confinement in the lateral direction increases, but this effect is smaller. In a thin dot (b) the wavefunction is flattened in the vertical direction because of the higher confinement, but now the lateral confinement is weaker.

5.1.2.2 The magnetic field perpendicular to the growth direction

Now the measurements on the dots with $B \perp z$ are discussed and compared with the QW results. In Figure 26 the PL energy as function of the magnetic field is plotted for the four QD-samples. Three samples have only a parabolic part, the same as for the QWs in this field direction, which indicates again the better confinement in this direction. On the other hand, for one sample, with barrier $D = 7$ nm, the curve behaves linearly in high fields, which could indicate that the confinement is weaker in this sample.

Another indicator for the confinement is the energy shift, which is given in Table 6 and is indeed the highest for sample 31, although for sample 33 almost the same shift is measured. These are both the thickest dots with a thin barrier, which could explain the weaker confinement is these dots. The energy shifts of the other two samples are the smallest, so the confinement is better in these samples with the thinner dots and thickest barriers.

For sample 31 the exciton radius and the mass can be calculated, which are 7.17 nm and 0.28 m_e, respectively. This big radius indicates again that the electrons are weakly confined. The minimum exciton radius for the other samples is estimated from the diamagnetic shift, supposing just as for the wells that the exciton mass equals 0.056 m_e. These estimated radii are given in Table 6 and are all smaller than the dot thickness, so the excitons would be well confined in the dots. A maximum radius is same as for the QWs, assuming that the crossover from parabolic happens at $B = 50$ T which gives a radius of 5.13 nm. The range on these minima and maxima is quite large and no conclusion about the

wavefunction spill over is possible, so another indication of the exciton radius would be useful. This is found by assuming that the exciton mass of sample 31 is also valid for the other samples and should be used to calculate the exciton radius. These values are also given in Table 6, and the radii are definitely close to the maximum radius of 5.13 nm for samples 26 and 24, which indicate that the wavefunctions spill over into the barriers. For sample 33 the calculated radius is even bigger than the maximum value. A possible explanation is that the curve behaves linear at the high field side, starting from 33 T, which is difficult to fit because the measurement is too noisy. We can conclude now that the exciton wavefunction spills over into the barriers, just as for the QWs, but that the spill over is the biggest in the samples with a thin barrier. This confirms again that the confinement is weaker in samples with a thin barrier.

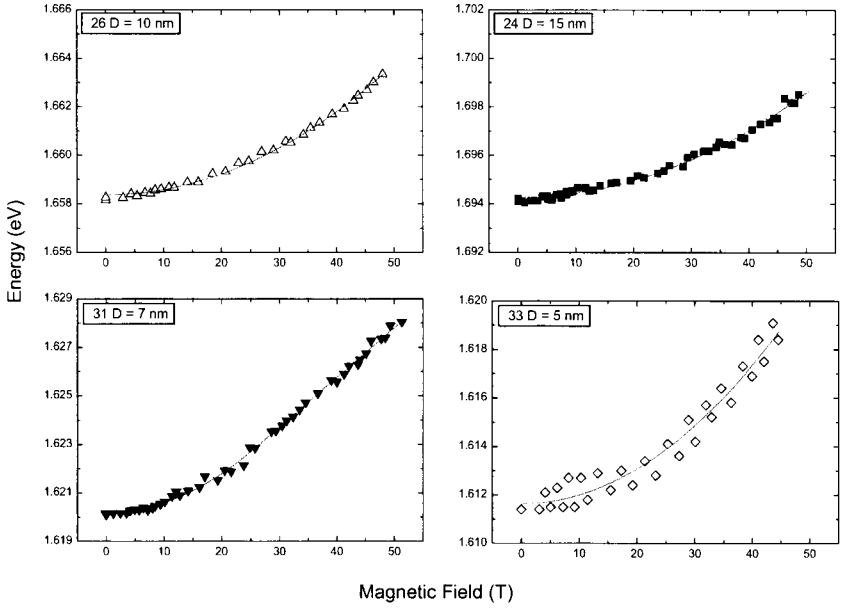

Figure 26: The PL energy is plotted as function of B with B⊥z for the four QD samples. The PL energy only has a parabolic behaviour for three samples and in one case, sample 31, the curve behaves linearly in high fields. The energy shift of the samples 26 and 24 is smaller than in the case of samples 31 and 33.

Another result to explain is the very high mass measured in sample 31. Until now the non-parabolicity of the energy bands was given as main reason for the high exciton masses. This gives a mass that depends inversely on the thickness of the quantum structure. This worked well to explain the in-plane masses of the excitons in the QDs, but is not enough to explain the value of 0.28 m_e in the z-direction. A possibility is that the overlap into the barriers is more important in this direction. The exciton diameter is 14 nm, which is more than twice the thickness of the dots, thus we suppose that the wavefunction spill over causes the electron mass to increase because the effective electron mass is higher in $Al_xGa_{1-x}As$.

Table 6: The PL data for the dots with B⊥z. The exciton radius for sample 31 is measured from the crossover field. The radii for the three other samples are calculated using two different values for the mass.

Sample No.	D (nm)	ΔE_{CM} (meV ± 0.5 meV)	Exciton radius (nm ± 0.2 nm)		QD thickness (nm)
			$\mu = 0.056m_e$	$\mu = 0.28m_e$	
33	5	7.7	2.8	6.3	6.30
31	7	8	-	7.2	5.76
26	10	5.1	2.3	5.1	5.32
24	15	4.3	2.1	4.7	4.36

The last thing to discuss with respect to these measurements is the intensity, which is plotted as function of *B* in Figure 27. Comparing this with the same graph for the QWs (Figure 21), in the case of the dots there is only one sample, no. 33, with an increasing intensity. This indicates that the tunnelling limit changes from 7 nm for the QWs to 5 nm for the dots. The dots are thicker than the QWs, so the energy level of the electrons is lower, which decreases the tunnelling probability. Again in high fields the PL intensity of all four samples become comparable, because the tunnelling is suppressed by the magnetic field.

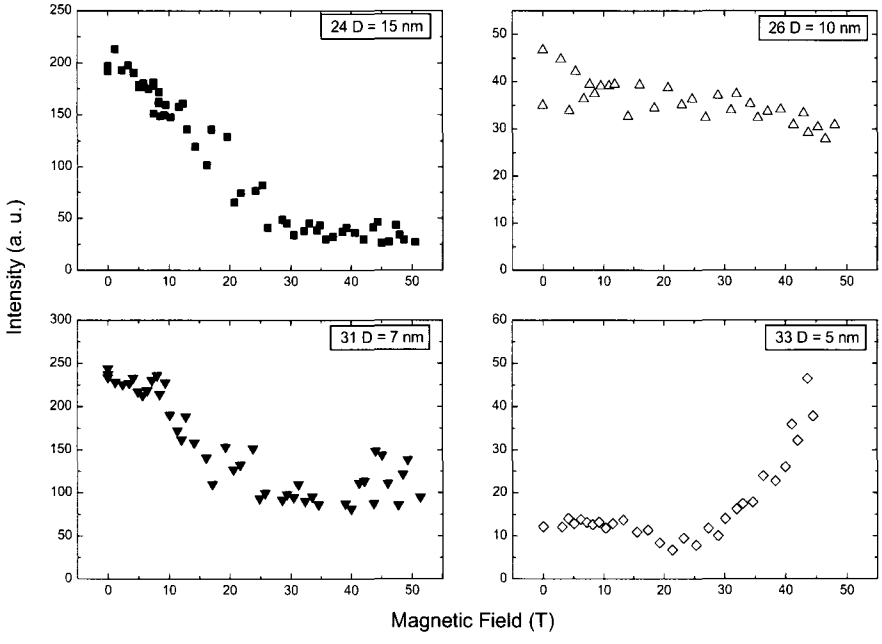

Figure 27: The intensity of the QD PL peak as function of B, with B⊥z. The intensity increases for sample 33, the one with the thinnest barrier. The intensity decreases for the other three samples.

5.2 Laser intensity dependent measurements

The dependence of the PL energy on the laser intensity is discussed in this last part. This dependence is measured for two types of QDs and for two QWs. For one QD sample it is also possible to measure excited states at higher laser intensity. These excited states are also studied with magneto-photoluminescence.

The discussion starts with the dependence of the PL energy on the laser intensity, which is plotted for the four cases in Figure 28. For the both QWs the influence of the intensity on the PL energy is small, but the situation for the dots is different. The PL energy of the dots depends strongly on the laser intensity, especially in the case of sample 31. The PL energy clearly decreases as function of the laser intensity for this sample. This dependence is already observed by Rastelli *et al* [6]. and explained by PL peaks, which can't be differentiated, appearing at the lower energy side. These peaks are biexiton and multiexciton lines, which become more intense than the exciton line when the laser intensity increases and so causes the energy shift of the ground state [26]. In the case of sample 26 the dependence is weaker and opposite.

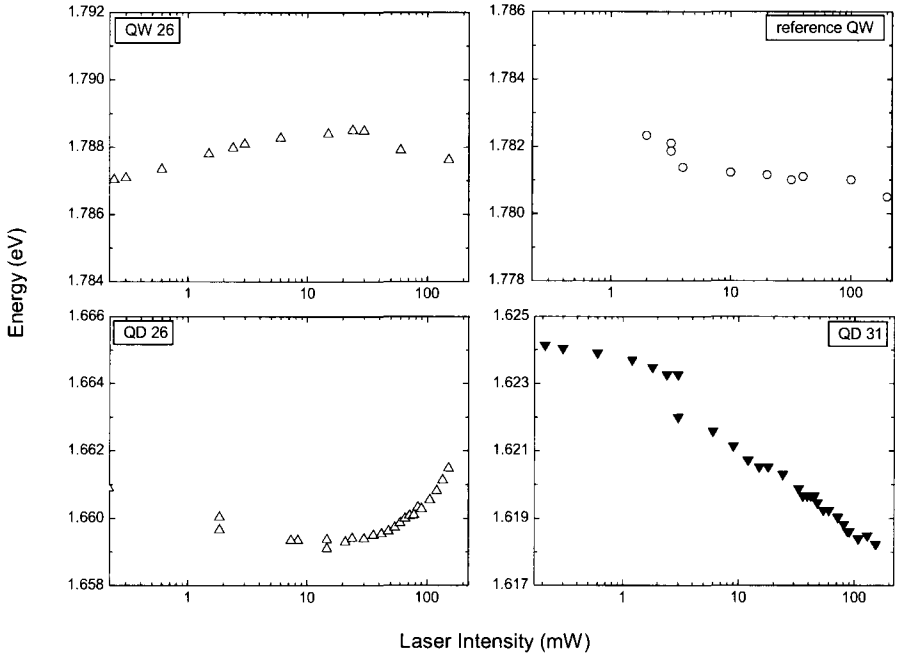

Figure 28: The dependence on the laser intensity for the QW of sample 26 and the reference QW are plotted in the upper half of the figure. The dependence for the QDs of samples 26 and 31 are plotted below.

In the case of sample 31 a second interesting thing is observed: excited states appear when the laser intensity increases. When the excitation intensity increases, then the ground state becomes saturated

and the first excited state will be filled up. A further increase of the excitation intensity causes the saturation of the first state and the filling of the second state, and so on. In practice the filling of the higher states starts before the ground state is saturated [11]. With the available laser power it is possible to measure the ground state and two excited states.

Magneto-photoluminescence measurements are done on this sample at different laser powers. For the ground state the exciton mass and radius are calculated each time, as given in Table 7. The radius and the mass are both a bit lower when three states are measured. In the case that two peaks are visible, then the radius is the biggest and also the energy shift is bigger. This indicates that the appearance of the excited states causes a decrease of the confinement of the ground state. The energy shift is the smallest when only the ground state is measured.

Table 7: The measured properties of the ground state as function of the laser power. Notice that the energy shift, and so the confinement becomes bigger when the excited states appear.

Laser power (mW)	**E_{CM} (eV ± 0.0005 eV) at $B = 0T$**	**ΔE (meV ± 0.5 meV)**	**Reduced mass ($m_e \pm 0.01\ m_e$)**	**Exciton radius (...nm ± 0.2 nm)**	**Number of peaks**
2.8	1.623	18.4	0.12	7.6	1
155	1.619	*22.3*	0.12	*8.0*	2
350	1.620	20.6	0.11	7.2	3
500	1.620	20.4	0.11	7.2	3

The PL intensity decreases as function of field, which is probably due to an increase of the recombination time in magnetic fields. However the intensity decreases much faster for the excited states, which seem to disappear in magnetic field, as shown in Figure 29. In high fields only the ground state is measured. The total PL intensity of the three states decreases in field, but when the two excited states are no longer visible, then the intensity of the remaining ground state stays constant and even increases a little bit at the highest fields. The PL energies as function of field are plotted in Figure 30 for the highest laser power. The error on the PL energy is higher for the excited states and becomes bigger when the field increases, because the peaks become too weak to distinguish. Therefore it is difficult to say something about the energy change of the second excited state.

Excited states in high fields up to 73 T are measured already by D. Smirnov et al. in the case of InAs/GaAs self-assembled QDs [27]. There are several remarkable differences between their measurements and graph shown here. First of all the energy difference between the ground state and the first excited state is only 17 meV, which is less than mostly found in QDs (typically around 40 meV). The difference between the first and the second excited state is a bit lower, 12 meV. The

total quantisation energy ΔE of the ground state is the PL energy minus the band gap. (Because the binding energy is negligibly small, the quantisation energy is almost the same as the confinement energy).

$$\Delta E = E_{PL} - E_g$$
$$\Delta E = 1.62\,eV - 1.52\,eV = 100\,meV \tag{5.1}$$

The measured quantisation energy for the ground state is much bigger than the energy difference between the first excited state and the ground state. The energy of the first excited state can be estimated by approximating the quantum dot potential by a parabolic potential, where the energy levels are equally separated. The estimated energy of the excited state is then the band gap plus two times ΔE.

$$E_1 = E_g + 2\Delta E \tag{5.2}$$

This gives an energy of 1.721 eV for the first excited state, while the measured energy is only 1.637 eV. A reason for this low energy could be that the measured state is not the first excited state, but the recombination of e.g. electrons in the ground state and holes in the first excited state. The quantisation energy is then only due to the holes and therefore these energy separations of the peaks are so small.

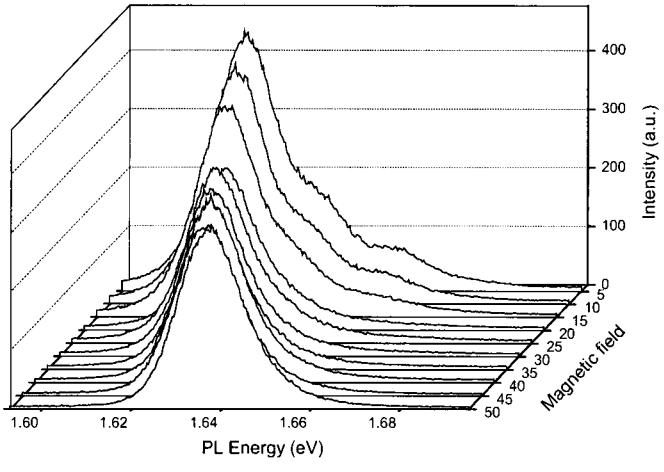

Figure 29: The Pl spectrum of sample 31 as function of the magnetic field. The ground state and two excited states are visible at zero field. When the magnetic field increases, then the excited states disappear and only the ground state is measured.

So, the measured excited states are probably not due to the recombination of the excited electrons and excited holes. According to this simple model, the p –state is expected to be at 1.72 eV, which is below the ground state of the QW and thus still confined in the dots. Nevertheless, this state doesn't

become visible when the excitation intensity increases, which can indicate that there are no electrons in the first excited state. The electrons, which are excited in the barriers, will fall in the QW and can move then from the well into the dots. However, instead of falling in the QDs, the electrons can tunnel out the well. The holes will also fall in the QW and then move into the dots, without the possibility to tunnel. This implies that more holes than electrons will fall in the dots and so that the excited hole-state is filled up while the excited electron-state stays empty.

Recombination of electrons and holes with a different principle quantum number n is forbidden due to the selection rules, so in principle it is unlikely to measure this recombination. However, in a system with finite wells with different depths for the electrons and the holes, this selection rule is less strict. All transitions between electron and hole states with the same parity are possible. When the well is asymmetric, then there is no restriction on the possible transitions. Nevertheless, in general the transitions with the same principle quantum number are the strongest [1]. In the measurements shown in Figure 29, it is indeed the case that the excited states are weaker than the ground state, but the measurements done by Rastelli *et al.* shows that the excited state becomes of the same intensity when the excitation intensity increases. Another possible explanation is that the radiative recombination is possible due to the emission or absoption of a phonon.

A second thing to notice is that there is no orbital splitting measured for the first excited state in high fields, while the second state is already visible. So, the reason is not that the first state is not completely filled. An explanation for the absence of the splitting can be that the splitting is now only caused by the holes. This splitting is smaller and probably not resolved. The PL-energy of the first state is almost constant up to 10 T, which can be an indication that it is an unresolved splitting state.

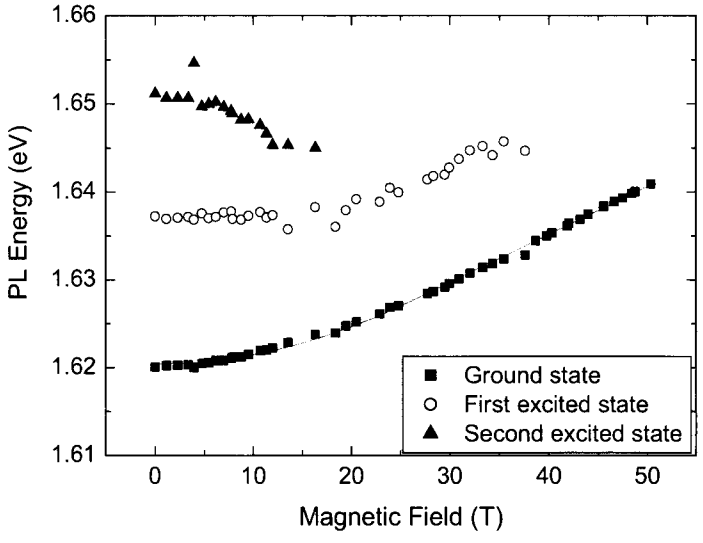

Figure 30: The PL energy as function of B for the three peaks. The two excited states become invisible when the field increases.

Conclusions

The GaAs/AlGaAs QD/QW system is studied in the first place as a model system that can be used for getting further insight into the fundamental properties of QDs. Here, we investigated the optical properties of these samples by photoluminescence in high magnetic fields and this method gives information about the exciton radius and mass. For both the QWs and the QDs the exciton masses measured with B//z are more than twice the value in bulk GaAs. The main reason for the increase of the mass is the non-parabolicity of the conduction band, which causes an unequal shift of the L-, the X- and the Γ-band in nanosize structures. The curvature of the Γ-band changes, which implies an increase of the electron mass. This effect becomes important in very small quantum structures and causes an inverse dependence of the mass on the structure size.

The production method makes it possible to tune the size of the QDs by changing the lower barrier thickness and thus to tune the emitted wavelength of the QDs. This tuning is limited due to poor confinement. When the lower barrier becomes too thin, the electrons can tunnel from the QW and QDs into the substrate, which will lower the PL intensity of the quantum structure. It is found that the tunnelling probability decreases by applying a magnetic field. The tunnelling can be avoided by using a higher Al concentration in the lower barrier to ameliorate the confinement. On the other hand, also when the barrier is thicker, the wavefunction spills over into the barrier. This indicates a poor confinement because the structure becomes very thin. So, in general the excitons are weakly confined in these dots, which can be a disadvantage of this production method.

This system can also be interesting to study excited states, which is done for one sample. The excited state measurements are not yet completely understood. A possible interpretation is that the measured states are forbidden transitions between the electron ground state and hole excited states. The intensity of measured excited states drops rapidly when an increasing magnetic field is applied. For a better interpretation of the excited state measurements, calculations will be helpful. Due to the negligible strain and intermixing and the good knowledge of the dot shape, it is possible to calculate the optical properties of this system. It is important that the non-parabolicity of the bands and the wavefunction spill over are taken into account, because it is found here that these two effects can influence the optical properties significantly.

References

(1) J. H. Davies, 'The physics of low-dimensional semiconductors', Cambridge University Press, (1998)

(2) F. Klopf, R. Krebs, J. P. Reithmaier, and A. Forchel, IEEE Phot. Tech. Lett. **13**, no. 8, 764 (2001)

(3) D. Bimberg, N.N. Ledentsov, M. Grundmann, F. Heinrichdorff, F.M. Ustinov, P.S. Kop'Ev, ZH. I. Alferov, and J.A. Lott, Solid-state Electronics 42, no. 7-8, 1433 (1998)

(4) H. Saito, K. Nishi and S. Sugou, Elec. lett. **37** (27), 1293 (2001)

(5) A. Holden, "An Industrial Perspective on Self-Assembled Nanostructured Materials", Bookham Technology PLC (2004)

(6) A. Rastelli, S. Stufler, A. Schliwa, R. Songmuang, C. Manzano, G. Costantini, K. Kern, A. Zrenner, D. Bimberg, and O.G. Schmidt, Phys. Rev. Lett. **92**, 166104 (2004)

(7) J. Maes, "Magneto-photoluminescence of self-assembled InAs nanostructures", Ph.D. thesis, KULeuven (2004)

(8) R. Provoost, "Magneto-photoluminescence of stacked quantum dots and stress analysis of melt-grown superconductors by Raman spectroscopy", Ph.D. thesis, KULeuven (2000)

(9) M. Hayne, J. Maes, S. Bersier, M. Henini, L. Müller-Kirsch, Robert Heitz, D. Bimberg, and V.V. Moshchalkov, Physica B **346-347**, 421 (2004)

(10) R. Rinaldi, P.V. Giugno, R. Cingolani, H. Lipsanen, M. Sopanen, J. Tulkki and J. Ahopelto, Phys. Rev. Lett. **77**, No. 2 (1996)

(11) D. Bimberg, M. Grundmann, N.N. Ledentsov, "Quantum dot heterostructures", John Wiley & Sons Ltd, 1999

(12) A.G. Steffan, R.T. Phillips, Physica E **17** (2003) 15-18

(13) F.E. Prins, G. Lehr, H. Schweizer and G.W. Smith, Appl. Phys. Lett. **63**, No. 10 (1993)

(14) T. Wang and A. Forchel, Appl. Phys. Lett. **73**, No. 13 (1998)

(15) A. Hartmann, Y. Ducommun, L. Loubies, Klaus Leifer, and E. Kapon, Appl. Phys. Lett. **73**, No. 16 (1998)

(16) R. Songmuang, S. Kiravittaya, and O. G. Schmidt, Appl. Phys. Lett. **82**, no. 17 (2003)

(17) H. Schuler, N. Y. Jin-Phillipp, F. Phillipp, and K. Eberl, Semicond. Sci. Technol. **13**, 1341 (1998)

(18) A. Franceschetti and A. Zunger, Phys. Rev. B **52**, No. 20, 14664 (1995)

(19) I. Vurgaftman, J. R. Meyer, and L.R. Ram-Mohan, J. Appl. Phys. **89**, No. 11 (2001)

(20) B. Koopmans, P.V. Santos, and M. Cardona, Phys Status Solidi B 205 (2): 419-463 (1998)

(21) J. Batey and L. Wright, J. Appl. Phys. **59**, No. 1 (1986)

(22) S. Wei, and A. Zunger, Appl. Phys. Lett. **72**, No. 16 (1998)

(23) J. Vanacken, Physica B **294-295**, 591 (2001)

(24) M. Städele and K. Hess, J. Appl. Phys. **88**, 6945 (2000).

(25) A. Polimeni, A. Patanè, R. K. Hayden, L. Eaves, M. Henini, P. C. Main, K. Uchida, N. Miura, J. Main, G. Wunner, Physica E **13**, 349, (2002)

(26) F. Findeis, A. Zrenner, G. Böhm and G. Abstreiter, Solid State Comm. **114**, 227 (2000)

(27) D. Smirnov S. Raymond, S. Studenikin, A. Babinski, J. Leotin, P. Frings, M. Potemski, A. Sachrajda, Physica B **346-347** (2004)